

**PRODUCTION AND MANIPULATION OF 2D DROPLET
AGGREGATES**

**PRODUCTION AND MANIPULATION OF
TWO DIMENSIONAL DROPLET
AGGREGATES**

By

SOLOMON BARKLEY, B.Sc.

A Thesis

Submitted to the School of Graduate Studies
in Partial Fulfillment of the Requirements
for the Degree
Master of Science

McMaster University

©Copyright by Solomon Barkley, 2015.

MASTER OF SCIENCE (2015)
(Physics)

McMaster University
Hamilton, Ontario

TITLE: Production and manipulation of two dimensional droplet aggregates

AUTHOR: Solomon Barkley, B.Sc. (McMaster University)

SUPERVISOR: Dr. Kari Dalnoki-Veress

NUMBER OF PAGES: [1](#), [49](#)

Abstract

This is a ‘sandwich thesis’ comprising three distinct research streams I have pursued during the course of my master’s degree. The first two streams have concluded, each resulting in a manuscript that is presented as a separate chapter of this thesis. The third research stream is ongoing, but preliminary results are presented in another chapter of this thesis.

The first research stream presented in this thesis concerns the development of a technique to produce droplets with diameters as small as $5\ \mu\text{m}$ with an extremely narrow size distribution in comparison to other methods. Other advantages of this technique, known as the snap-off method, include its simplicity and ease of tuning droplet size. The results of this research are presented in chapter 3 in the form of a manuscript that is currently in press.

The second research stream of this thesis explores the physics that drive droplet snap-off. A model was developed to predict the size of droplets, dependent on fluid properties, system geometry, and fluid flow rate. Experiments examined each of these parameters in turn, providing a cohesive understanding of the mechanism behind droplet snap-off. Multiple unanticipated predictions of the model were also verified experimentally. This research is presented in chapter 4 as a manuscript that will be submitted shortly.

The final research stream of this thesis investigates forces in emulsions as they relate to a transition from glassy to crystalline dynamics. Specifically, 2D aggregates of droplets were compressed with micropipettes, providing both imaging of cluster evolution, as well as the force applied during compression. This research stream has demonstrated qualitative differences between droplet clusters that differ in composition so as to behave like crystals, glasses, or intermediate states. More quantitative analysis is required before this research stream is ready to be published. Preliminary results are presented in chapter 5.

Acknowledgements

First of all, I would like to thank my parents and brothers for always expressing interest in my research and encouraging me to realize my full potential. Not only do they put up with me studying on family vacations, but they ask me to present conference talks for them and to show them around the lab when they visit Hamilton. This active engagement with what I do every day means a lot. While on the subject of family, I'd also like to mention my late grandfather, who provides a source of inspiration as I embark on an academic career. Finally, Rachel is the one who has had to deal with me on a daily basis during my master's work, and rarely gets the recognition she deserves. I do appreciate the sacrifices she has made on my behalf over the past two years.

I owe a lot to my colleagues and friends in the lab as well: Paul, Raffi, Matilda, Mark, Rob, and Adam. Each of them has taught me a lot over the course of my master's degree, both in terms of science and about life in general. I am grateful for the heated discussions about mundane subjects, the various sports and athletic pursuits, and all of the time spent together. I hope we keep in touch over the years to come.

Most importantly, I cannot sufficiently express my gratitude to my supervisor, Kari Dalnoki-Veress. During my first week of grad school, he won the President's award for excellence in graduate supervision, and I have experienced this 'excellence' first hand over the past two years. As I began investigating PhD options, I had to come to terms with the realization that no other supervisor could live up to the unreasonable standard I was used to. Kari cares deeply about his students' well-being and success, and his excitement about research is contagious. This thesis, the research it contains, and my future aspirations would all be much less interesting if not for his influence and guiding hand. In short, Kari has taught me what it means to be a scientist and a mentor.

Contents

Abstract	iii
Acknowledgements	iv
1 Introduction	1
1.1 Emulsions	2
1.2 Microfluidics and droplet production	4
1.3 Forces in emulsions	6
2 Experimental Details	11
2.1 Micropipettes	11
2.2 Experimental Setup	13
2.3 Droplet Clusters	16
2.4 Image processing and analysis	17
3 Snap-off production of monodisperse droplets	21
4 Predicting the size of droplets produced through Laplace pressure induced snap-off	27
5 Compression of two-dimensional droplet clusters	35
6 Conclusions	43

CONTENTS

List of Figures

1.1	Illustration of complex emulsions, with the continuous phase in blue, surfactant layer in red, and dispersed phases in orange and yellow. A) Emulsion with two distinct dispersed phases. B) Emulsion of Janus droplets. C) Double emulsion.	4
1.2	Illustration of droplet production techniques, with the continuous phase in blue, surfactant layer in red, and dispersed phase in orange. A) T-junction emulsification. B) Co-flow emulsification C) Laplace-pressure emulsification in a stepped geometry.	6
1.3	Illustration of the depletion interaction. Depletant particles (dark blue) cannot overlap with droplets (yellow) and so a depletion zone exists around droplets (black dashed lines) where the centres of mass of the depletant particles cannot be found. If these depletion zones overlap, particles will not fit between droplets, and the droplets are entropically forced together to maximize mixing of exclusion particles and the continuous phase molecules.	8
2.1	A) Schematic of the sample chamber and pipette assembly (side view). B) Top view of half of the sample chamber with pipettes used for cluster compression experiments. C) Pipettes enter the centre of a filled chamber. D) Pipettes are drawn to the top and bottom coverslips if some solution has evaporated.	14

LIST OF FIGURES

2.2 Effect of condenser lens position on images. A) Condenser moved to the top of its range. B) Aligned condenser. 18

5.1 Experimental setup for compression of droplet clusters. A) Top view. The stiff pipette on the left is pushed forward at a constant rate, while the flexible pipette on the left deflects in response to applied forces. B) Side View. Droplets float to the top of the sample chamber. 37

5.2 Compression of a monodisperse droplet cluster. A) Cluster is crystalline prior to compression. B) The crystal can withstand some force, and the lower flexible pipette deflects. C) Force increases past the breaking point of the crystal, and it fractures. D) The droplets slide easily past one another after breaking apart. E) The droplets eventually achieve a new crystalline configuration. F) Deflection of the lower pipette plotted against cluster compression (blue curve) during the entire experiment. Data points corresponding to the images in panel A-E are indicated by red letters. 38

5.3 Effect of crystal boundaries. A) One large crystal. Upon compression, the droplets can only displace from its ends. B) Two smaller crystals. Upon compression, the droplets can displace from the ends or into the middle of the structure. C) Force-compression curve of the clusters shown in panel A (blue curve) and B (red curve). Black arrows indicate a longer relaxation time of the large crystal as droplets move further. 39

5.4 Bidisperse droplet cluster, with smaller droplets indicated in red and larger droplets in blue. A) Prior to compression, droplet arrangement is not as well ordered as the monodisperse droplets in Figs. 5.2 and 5.3. B) Force-compression curve of the bidisperse cluster has many irregularly spaced peaks of varying heights due to its chaotic breakup. 40

5.5 Force curves of droplet clusters containing single defects. A) A single droplet larger than the others in the clusters causes one region of the crystal to locally fracture at lower compression than the rest of the crystal, indicated by black arrows. B) if the defect droplet is abnormally small, it shifts fracture to a higher compression, indicated by black arrows. 41

Chapter 1

Introduction

Everyone is familiar with liquid drops, and understands intuitively that they differ from both bulk liquids and small solid particles. If I asked someone to present me with some droplets of liquid, they would not see this as a difficult task. If I insisted that all droplets be exactly the same size, or that they be arranged in some particular configuration, this would likely elicit some questions from my audience, but my request could be fulfilled without too much effort. If I further specified that the droplets had to be smaller than the diameter of a hair, the task would soon become impossible without specialized equipment. The best I could hope for would be a fine spray or mist, with no guarantees regarding droplet size or arrangement. The challenge of transitioning from macroscopic to microscopic droplets is not merely a matter of smaller movements and increased magnification. Instead, entirely different physics come into play at micrometric length scales, as weight and inertia give way to viscosity and surface tension as the dominant forces driving the evolution of a system. Conventional macroscopic techniques, no matter how reliable and precise, simply will not work at a microscopic length scale.

The transition from macroscopic to microscopic regimes is often described through the introduction of dimensionless numbers. A common example is the Reynolds number, which describes the ratio of inertial to viscous forces in a system. Similarly, the ratios of both inertia and weight to surface tension forces are captured by the Weber and Bond numbers, respectively. In the case of microscopic droplets, each of these numbers becomes vanishingly small. Because we are used to an environment where

these numbers are large, it can often be counterintuitive to interpret and understand systems on micron length-scales.

1.1 Emulsions

An emulsion is a system consisting of liquid particles (droplets) immersed in a liquid matrix, just as a mist consists of liquid particles in a gaseous matrix. Emulsions are critically important for industrial applications, specifically regarding foods, cosmetics, and petroleum products. Often, the most fragrant and active ingredients in foods and cosmetics are not water-soluble. Emulsions provide a convenient way to deliver these compounds in a biocompatible, aqueous format [1]. Petroleum products are often extracted and transported as emulsions, either unintentionally or intentionally [2].

The two liquids composing an emulsion must be immiscible, as they would otherwise mix to form a single liquid phase. The liquid forming the droplets of an emulsion is referred to as the dispersed phase, while the liquid forming the matrix is referred to as the continuous phase. Additionally, emulsions composed of water droplets in oil, or oil droplets in water, are often referred to as W/O and O/W emulsions, respectively. Emulsions are physically distinct from foams or suspensions, which contain either gas or solid particles dispersed within a continuous liquid phase. Unlike solid colloidal particles, emulsion droplets are deformable, which becomes especially important at high volume fractions of the dispersed phase as droplets are squeezed together [3, 4]. Additionally, the droplets within an emulsion are dynamic at a molecular scale, and are able to exchange material with neighbouring droplets without ever coming into contact by diffusion of individual dispersed phase molecules through the continuous phase [5].

Emulsions are inherently unstable over arbitrarily long timescales [5]. The two liquids have some interfacial tension γ , which represents the energy cost per unit area of maintaining an interface between two materials. Typical interfacial tensions for liquids producing relatively stable emulsions are on the order of 5 mJ/m² or 5 mN/m [5]. Initially, this may seem like a relatively small energy cost, especially in comparison to the surface tension of water, at 72 mJ/m² [5]. However, emulsions are remarkable for containing so much surface area that the total energy cost of the

emulsion ends up being rather large. Consider a one litre carton of homogenized milk, where fat globules range in size from < 50 nm up to ≈ 500 nm radius [6]. Butterfat density is roughly 900 kg/m^3 and fat concentration of homogenized milk is 3.25% by weight, so we expect a total of 36 mL of fat in the milk [7]. If globules have a radius of 100 nm, there must be 8.6×10^{15} fat globules in the milk. These have a combined surface area of slightly more than $10,000 \text{ m}^2$. If interfacial tension is 5 mJ/m^2 , then the total surface energy in the milk is 50 J. This is roughly equivalent to the gravitational potential energy of the same litre of milk suspended two stories above the ground.

All of this energy could be released if the fat globules within the milk were able to coalesce. Most emulsions require a stabilizing agent in order to prevent coalescence of the dispersed phase. In the case of milk, this role is filled by casein protein molecules [6]. In a laboratory setting, it is often simpler to use surfactant molecules. These amphiphilic molecules stabilize the emulsion by aggregating at the interface, reducing the interfacial tension from $\approx 50 \text{ mN/m}$ to $\approx 5 \text{ mN/m}$, which was the value used in the above example [8,9]. Because the surfactant molecules interact favourably with both phases, they form an intermediate layer that reduces the total energy cost of maintaining the interface and prevents coalescence of individual droplets. This idea can be taken one step further with Pickering emulsions, where small solid particles mediate the interface between the two phases instead of surfactant molecules. Even though two interfaces are created by the introduction of small particles, both can be much more favourable than the direct contact of the two liquid phases, and so the total energy cost can be lower than if the solid particles did not accumulate at the interface [10].

It is also possible to produce more complex emulsions with multiple dispersed phases within a single continuous phase (Fig. 1.1A) [11]. Going one step further, the emulsion droplets can be Janus particles, with two separate liquid phases that share a common interface (Fig. 1.1B) [12]. Finally, droplets of dispersed phase can themselves be emulsions, with another dispersed phase inside them, which is termed a double emulsion (Fig. 1.1C) [1, 13]. Oil-in-water-in-oil (O/W/O) and water-in-oil-in-water (W/O/W) are the most common examples of this type of emulsion. There are other possibilities for emulsions with a more complex hierarchical structure. For example,

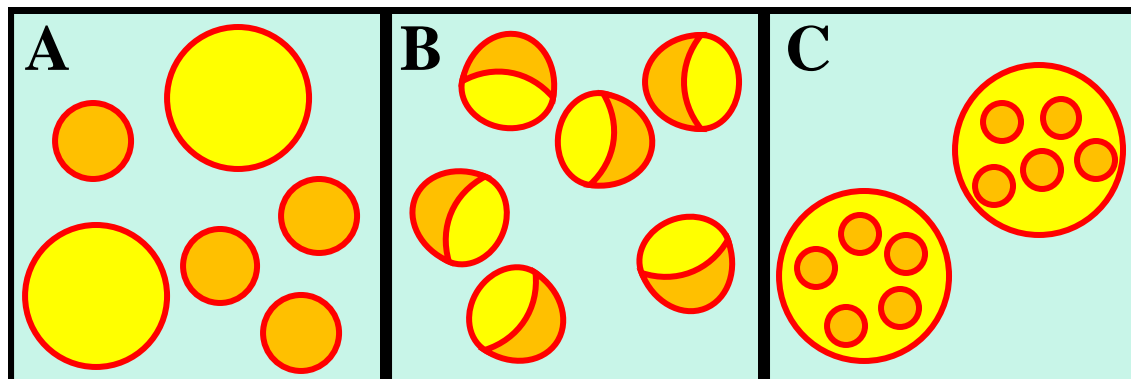


Figure 1.1: Illustration of complex emulsions, with the continuous phase in blue, surfactant layer in red, and dispersed phases in orange and yellow. A) Emulsion with two distinct dispersed phases. B) Emulsion of Janus droplets. C) Double emulsion.

the emulsion droplets can be filled with small colloidal particles, or droplets of a third immiscible fluid, giving rise to rich and unexpected phenomena [4, 14].

1.2 Microfluidics and droplet production

Part of the push to develop and understand emulsions comes from the advent of droplet microfluidic technologies. These devices use precise control to manipulate individual emulsion droplets in order to accomplish specific biological or chemical tasks. For example, droplets containing different chemical compounds can be steered in a desired direction and combined, giving researchers precise control over where and when a desired chemical reaction takes place [11]. Performing a reaction in this way allows for improvements to reaction selectivity and yield, in addition to finer control over external reaction parameters, such as temperature, as compared to a bulk reaction [13]. Droplet microfluidics hold particular promise for situations in which it is advantageous to perform similar steps on many individual droplets with distinct contents. High-profile examples include DNA sequencing, screening individual cells for disease, or testing activity of a chemical library of related compounds [15–17].

Attaining these goals requires development of many tools to efficiently manipulate individual droplets. Specifically, droplets must be directed, identified, sorted, stored, joined, and separated. All of these tasks must be performed automatically and reliably by the microfluidic device. In order for many microfluidic techniques to be useful,

they must be able to process droplets quickly, often at rates of 10^5 droplets per second [13]. This is necessary in order to achieve reasonable volumes in the case of chemical reactions, and to test high numbers of unique droplets for screening and sequencing purposes [13]. Additionally, it is important that droplets be uniform in size to maintain concentrations across droplets and to ensure high fidelity processing of droplets as they move through the microfluidic device.

Many different techniques have been developed to produce droplets with a narrow size distribution, or high monodispersity. Typically, monodispersity is measured as the coefficient of variation (CV) in droplet radius, defined as the ratio of radius standard deviation to mean droplet radius. Several techniques relying on different physical mechanisms have been shown to produce droplets with $CV \leq 2\%$ [11, 12, 18, 19]. One of the most popular for microfluidic devices is T-junction droplet production, depicted in Fig. 1.2A. A channel containing flowing dispersed phase (orange) joins another channel containing the flowing continuous phase (blue), which causes the dispersed phase to break up into discrete droplets [20]. Another broad category of droplet production mechanisms are those that rely on co-flow of the dispersed and continuous phases, depicted in Fig. 1.2B. In this case, the dispersed phase is not directly in contact with any boundaries, but breaks into droplets to minimize interface with the continuous phase, according to Plateau-Rayleigh instability [18]. By breaking into droplets, the total interfacial area is reduced as compared to a high-aspect ratio column of dispersed phase. A third category of droplet-production techniques relies upon chamber dimensions to impose differences in Laplace pressure (see sect. 1.3) across the interface between the two phases. Fig. 1.2C shows the dispersed phase being released from a channel onto a broad but shallow plateau, and forming droplets at two sites when the plateau floor gives way to a deeper chamber [21]. In each of these three droplet formation mechanisms, interfacial tension drives the dispersed phase to form droplets in order to reduce the total interface surface area. It is thus useful to compare dimensionless numbers that relate interfacial tension to other driving forces, such as inertial effects or viscous effects, captured by the Weber number and capillary number, respectively [18, 22]. Although the different droplet production methods operate over a range of capillary numbers, co-flow droplet production is restricted to high Weber number (high velocity), and Laplace-pressure driven droplet

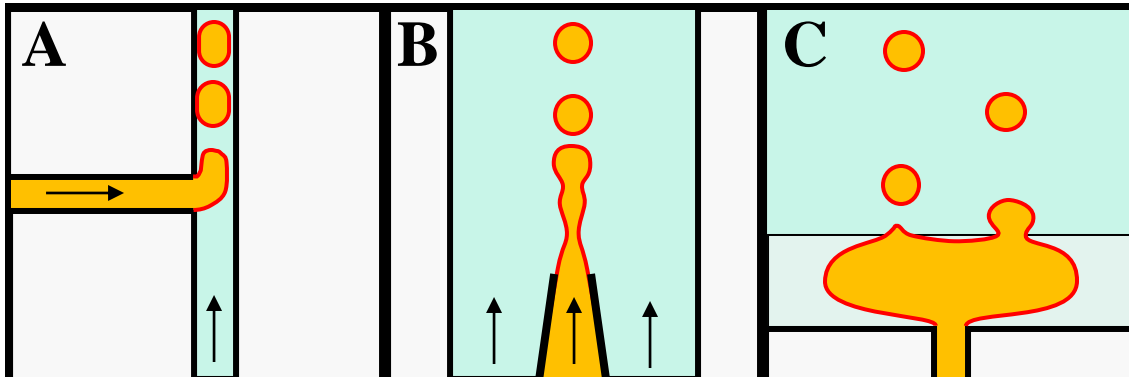


Figure 1.2: Illustration of droplet production techniques, with the continuous phase in blue, surfactant layer in red, and dispersed phase in orange. A) T-junction emulsification. B) Co-flow emulsification C) Laplace-pressure emulsification in a stepped geometry.

production is limited to low Weber number (quasi-static flow) [11, 18].

1.3 Forces in emulsions

Besides microfluidics applications, there is significant basic-science interest in emulsions and colloidal suspensions for their role in elucidating jamming and glass transitions. Like molecules, colloidal particles can exist in liquid, crystalline, or glassy states, depending on the packing density of particles, their mobility, and their spatial arrangement. Colloids have been used extensively to probe jamming transitions, since they are subject to similar physics as their molecular counterparts, but are much easier to study experimentally at a single-particle level [14, 23]. As colloid packing density (or interparticle attraction) increases past some critical value, the system jams and particle mobility decreases dramatically [23]. Emulsions provide an even closer analogue to a molecular glass, since droplets are deformable and so do not obey a hard-sphere repulsion like most colloids [3]. At a microscopic level, glasses are characterized by mobility of individual particles and cooperative motions during rearrangements [3, 24]. In a bulk system, one of the easiest ways to characterize a glass transition is through mechanical properties, since this is ultimately what distinguishes a glass from a viscous liquid [3, 25, 26].

Relevant mechanical properties include elastic and shear moduli, length and mag-

nitide of force chains, pressure, and the presence of free boundaries [3, 23–26]. Direct measurement of forces is thus a key experimental tool to deciphering the dynamics of glassy emulsions. There are two types of forces present in these systems: those due to deformation of droplets, and those due to interactions between droplets. Droplets in isolation are spherical so as to minimize the interface between the two phases. Any deviation from a spherical shape is highly unfavourable due to the interfacial tension between the two phases γ , which acts to pull the interface back into a spherical shape. This constant inward tension is balanced by the Laplace pressure of the droplet, given by

$$P_L = \frac{2\gamma}{R}, \quad (1.1)$$

where R is the droplet radius. It should be noted that P_L is not an absolute pressure, but a pressure difference, corresponding to the increase in pressure of the droplet interior relative to the droplet exterior. If a droplet is subjected to external stresses, its shape will deviate from a sphere and its boundary will not have uniform curvature [3]. However, a droplet in equilibrium must maintain uniform pressure, or else its contents will redistribute to ensure that this is the case. A droplet under compression experiences an increased inwards force that must be counteracted by its internal pressure, and so there is a larger pressure difference across the droplet boundary. Similarly, there is a smaller pressure difference across the boundary of a droplet under tension, as the tensile external force partially counteracts the forces exerted by interfacial tension. For relatively small external forces, droplets behave elastically and portions of its interface that are not directly influenced will maintain equal radii of curvature along different axes. This radius goes according to Eq. 1.1, with the total internal pressure replacing P_L [3].

In addition to the forces within droplets, emulsions are also governed by the forces between droplets, which can be attractive or repulsive. Generally, repulsive interactions are preferable to promote emulsion stability and prevent aggregation of droplets [5]. However, in their simplest form, emulsion droplets are attracted to one another through van der Waals interactions, and will aggregate over long timescales [10]. Many surfactant molecules are charged, and endow the droplets with a net charge if their counterion is dissolved in an aqueous continuous phase. The resulting electrostatic repulsion between droplets can be mediated through addition of

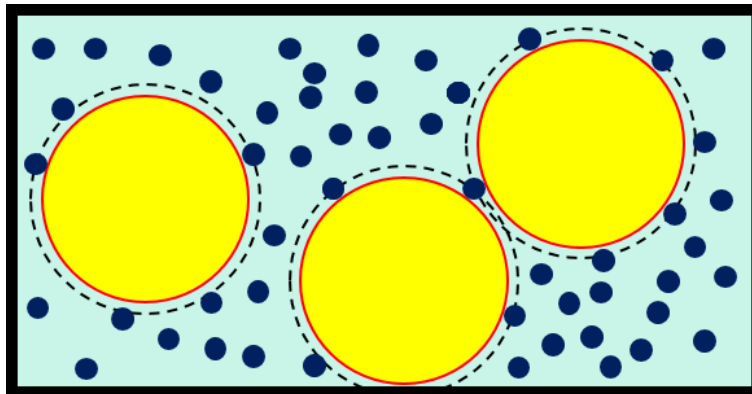


Figure 1.3: Illustration of the depletion interaction. Depletant particles (dark blue) cannot overlap with droplets (yellow) and so a depletion zone exists around droplets (black dashed lines) where the centres of mass of the depletant particles cannot be found. If these depletion zones overlap, particles will not fit between droplets, and the droplets are entropically forced together to maximize mixing of exclusion particles and the continuous phase molecules.

other salts to the continuous phase [23]. Other dissolved ions will screen the droplets' mutual repulsion and reduce the effect of charged surfactant molecules. It is also possible to elicit an attractive interaction between droplets through addition of a depletant, usually a polymer molecule or colloid particle much smaller than the emulsion droplets [5, 23]. A depletion layer is established around droplets, where the centres of mass of the depletant particles cannot be found due to excluded volume with the droplets themselves (dashed lines in Fig. 1.3). If droplets come close enough that their depletion zones overlap, no depletant particles will fit between the droplets, and the droplets are pulled together due to osmotic pressure. Entropy favours uniform mixing of the depletant particles within the continuous phase, and more configurations are possible if the droplets are brought into contact instead of merely being in proximity to one another. The distance over which the depletive attraction between droplets becomes important scales with the size of the depletant particles [23].

If we consider droplets of $R = 10 \mu\text{m}$ with $\gamma = 5 \text{ mN/m}$, Eq. 1.1 gives $P_L = 1 \text{ kPa}$. If this pressure is applied over a square patch of the droplet with side length equal to the droplet's radius, it exerts a force of 100 nN. The van der Waals force between two such droplets is given by $F = AR/12D^2$, with the Hamaker constant $A = 5 \times 10^{-20} \text{ J}$ for hydrocarbons and droplet separation $D = 0.2 \text{ nm}$ for droplets in close contact

[27]. This gives a force of roughly $1 \mu\text{N}$ to separate the droplets. Measurement of the mechanical properties of an emulsion therefore requires force measurements with a precision of 100 nN or less in order to probe the forces within and between droplets [3, 28]. While atomic force microscopy (AFM) is able to capture forces between individual droplets, it is not practical for bulk measurements or aggregates of several droplets, where the length scales and forces are larger than are suitable for AFM [28].

One technique to measure forces in this range is micropipette deflection. Thin ($\approx 20 \mu\text{m}$) glass tubes are used as cantilevers with spring constants on the order of $100 \text{ nN}/\mu\text{m}$ [29]. Deflections of the micropipettes are observed through an optical microscope or recorded with a reflected laser to provide a direct measurement of the applied force [29, 30]. This method is particularly useful for biological and soft samples, and has been previously applied to delicate samples such as living cells, swimming organisms, and polymer shells [29, 31, 32]. Suction through the pipette can be useful for holding samples in place and aligning them prior to recording a measurement. The pipettes can be shaped to achieve a desired stiffness and direction of force measurement relative to the orientation of the micropipette tip [32]. Details regarding the application of micropipette deflection to the present study will be discussed in section 2.1.

This thesis focuses on two different problems related to emulsion physics. First, a novel technique was developed to produce monodisperse droplets that offers advantages over other methods. Second, micropipettes were used to conduct direct force measurements of droplet clusters under compression, while cluster dynamics were simultaneously imaged. The first problem was motivated by the development of microfluidic technologies, while the second aims to probe the jamming transition. Experimental details of both projects are described in the next chapter. Chapter 3 outlines the snap-off method of droplet production and describes its implementation to produce a variety of droplets. The physics of snap-off droplet production are further explored in chapter 4. Finally, chapter 5 presents preliminary results on compression of 2D droplet clusters, probing a transition from glassy to crystalline dynamics based on cluster organization.

Chapter 2

Experimental Details

Chapters 3, 4, and 5 contain descriptions of their associated experiments to permit complete understanding and interpretation of their results. This chapter provides additional technical details that would be helpful for others pursuing similar experiments. Emphasis is on points that do not appear in chapters 3, 4, and 5.

2.1 Micropipettes

Glass capillary tubes of 1 mm outer diameter and 0.54 mm inner diameter (World Precision Instruments, USA) were stretched into micropipettes using a PN-31 pipette puller (Narishige, Japan). This device fixes either end of the capillary tube, with its centre passing through a tube formed from a bent ribbon-shaped platinum filament. Current is passed through the filament, providing uniform heating around the capillary tube over a short portion of its total length and melting it in this region. Simultaneously, the ends of the capillary tube are pulled apart by an electromagnet, with a step increase in pulling strength after the ends have been separated by a fixed threshold distance. The rapid pulling enables production of pipettes that taper significantly over a short range and then maintain a nearly constant diameter (of order 10 μm) over a length of several centimetres. Degree of heating, as well as both magnet steps can be adjusted on 0–100 scales. Typical parameters used to produce long, thin micropipettes were heating 92.1, magnet-sub 14.8, magnet-main 56.1. Generally, increased heating produces longer pipettes. However, if the heating is too high, the

glass thread does not break over the entire range of motion of the pipette puller, and must be severed manually, which produces a thicker pipette with an open tip. Magnet-sub can be used to fine-tune the length and tip shape of the pipette at a given heater value, with larger values producing pipettes that are shorter and wider. Magnet-main was not adjusted extensively, and appears to have little effect on the pipettes. Unfortunately, the same settings do not always produce identical pipettes, although they are usually consistent within one pulling session of several pipettes. Additionally, the parameters depend on the exact position of the platinum filament and must be adjusted if the filament is disturbed or replaced.

It is often convenient to bend pipettes from their original straight linear shape. Current is increased through a 0.5 mm platinum-iridium wire (Alfa Aesar, USA) until the wire glows a dull red. When a pipette is brought into contact with the wire, it melts locally, and can be bent around the wire by applying a force to the end of the pipette. The pipette is then removed from the wire, and can be realigned to perform another bend in a different location, along a different axis. Pipettes with complex three-dimensional shapes for customized applications can be produced through sequential bends.

As a result of pulling, the tip of the pipette is sealed by glass. The tip of the pipette must be removed if the pipette is to be used for fluid ejection or suction. Even if the pipette is not to be used for these purposes, the extreme tip is typically bent at some angle relative to the rest of the pipette, and can interfere with pipette alignment if not removed. One method to remove pipette tips is to break the glass through sudden cooling. The pipette tip is tightly wrapped around a heated wire, as in the bending procedure described above. Current through the wire is suddenly removed, dropping its temperature below the melting temperature of glass and causing the pipette to break due to rapid thermal contraction while it still wrapped around the wire. This type of break is time consuming, but produces a ‘clean’ cut smoothly across the pipette. Pipette tips can also be broken by clipping with a pair of tweezers. This is much faster, but the pipette tip shape cannot be controlled, and is usually quite jagged. However, the same tip can be clipped many times until a desired shape is achieved.

Pipettes being used for force measurements must be calibrated to convert observed

deflections into applied force. All pipettes used for force measurements were calibrated by comparing their stiffness to that of a pipette with known stiffness. These earlier pipettes had been calibrated by measuring their deflection in response to the weight of water droplets of known volume, which confirmed the Hookean deflection of the pipettes [33]. These pre-calibrated pipettes were used in turn to calibrate the ones used for the present study, whose geometry prevented direct calibration with water droplets. The previously calibrated pipette was slowly pushed into the new pipette at a constant rate using a LTA-HS motorized actuator (Newport, USA). Images of the two pipettes were recorded and pipette deflections were measured (see section 2.4). Attempts were made to match the stiffness of the reference pipette to that of the one being calibrated, so that their deflections were similar in magnitude. Typical spring constants of the pipettes used in this study were ≈ 500 pN/ μm .

Pipettes were also pulled manually over an ethanol flame in chapter 3. Gradual pulling permits stretching of extremely long, thin pipettes that could be useful for force measurements. However, it was not possible to maintain completely coaxial pulling, and so these long pipettes were sealed shut with glass and could not be used for suction or ejection of fluid. Fast pulling produced hollow pipettes with more variation in dimension, presumably due to the difficulty in maintaining a constant temperature. In addition to manually pulled pipettes, chapter 3 also required coating pipettes with polystyrene (PS) for production of inverted water-in-oil emulsions. A high concentration ($> 10\%$) solution of PS in toluene was required to deposit a sufficient layer to change wettability by oil and water. High molecular weight solutions at this concentration are quite viscous, and while effective, they significantly change the tip geometry, often depositing a large mass of PS at the tip. Low-molecular weight solutions produce an even layer of PS on pipette tips. However, this layer is easily removed through contact with surfaces or heating during bending, so it is important that coating with PS be the final step in pipette production.

2.2 Experimental Setup

Sample chambers, depicted in Fig. 2.1A, were prepared by clamping two 22×40 mm glass coverslips (VWR,USA) separated by spacers cut from rubber tubing (brown

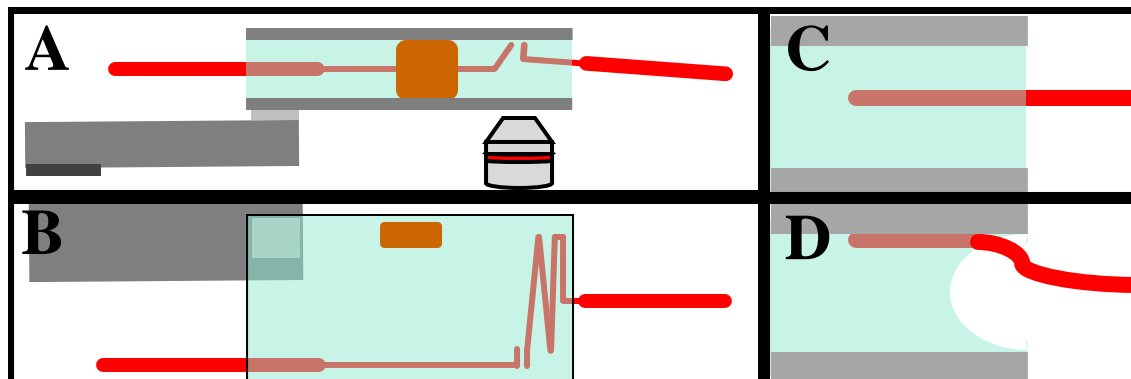


Figure 2.1: A) Schematic of the sample chamber and pipette assembly (side view). B) Top view of half of the sample chamber with pipettes used for cluster compression experiments. C) Pipettes enter the centre of a filled chamber. D) Pipettes are drawn to the top and bottom coverslips if some solution has evaporated.

rectangle in Fig. 2.1A). The two coverslips were adjusted until they were parallel, separated by a gap of ≈ 2 mm. The bottom coverslip of the sample chamber was affixed with double sided tape to a larger slide, which was held stationary on the microscope stage with adhesive magnetic ribbon. The double-sided tape was always completely covered by the coverslip so as to prevent leakage of sample chamber contents. The sample chamber was filled with an aqueous solution, held between the two coverslips by capillarity. The sample chamber was filled as much as possible to maintain a flat air-water interface around the boundaries (Fig. 2.1C). Otherwise, inserted pipettes are pulled to either coverslip to minimize the surface area of the air-water interface (Fig. 2.1D). Over time, water evaporated from the sample chamber, reducing total volume and increasing the concentration dissolved components. Between experiments, the sample chamber was refilled using deionized water if there was a substantial change in volume, on the order of a few percent of total volume. Every refilling event carried the risk of knocking or overfilling the chamber and causing it to leak, and so refilling was not performed unless deemed necessary to maintain experimental consistency.

Micropipettes entered the sample chambers from the sides (red structures in Fig. 2.1A and 2.1B), and their motion could be controlled in three dimensions with micromanipulators. To produce emulsions, mineral oil was forced into the pipettes with a syringe and acted as the dispersed phase when ejected from the pipettes. The

continuous phase was an aqueous solution with 1% sodium dodecyl sulphate (SDS) surfactant. This is above the critical micelle concentration at which the oil-water interface becomes saturated with SDS and changes to SDS concentration do not affect the interfacial tension γ . For many experiments, various other components were added to the aqueous continuous phase. SDS precipitates out of solution at glycerol concentrations in excess of 60% or sodium chloride (NaCl) concentrations greater than $\approx 3\%$. Pipettes being used to produce emulsions were kept far from the upper and lower coverslips comprising the sample chamber, as proximity to these surfaces influenced the size of emulsion droplets produced. However, the orientation (tilt and rotation) of the pipette tip did not affect droplet production, and so this was not controlled for between experiments.

Exceptionally narrow pipettes were used to produce droplets small enough to be influenced by Brownian motion in chapter 3. These pipettes were produced by increasing the magnet-sub setting on the pipette puller, resulting in pipettes with an additional tapered section at their tip, going from the already tapered $\approx 10 \mu\text{m}$ radius to $< 1 \mu\text{m}$ radius. The end of this narrow section was broken off by simply pushing the pipette tip against a solid object with a micromanipulator. Forcing oil along the length of the pipette was not an option for such small pipettes, as the viscosity of air prevented rapid flow through such a narrow opening (since Poiseuille flow rate goes with R^4). Instead, the pipette tip was left submerged in mineral oil for 40 hours and oil was drawn into the pipette through capillary forces. High pressures were required to force these droplets out of the pipette, and so only a few droplets could be produced at a time. When working with pipettes of this size, it is important to keep the tip submerged in a liquid, as air that enters the tip cannot be removed and renders the pipette useless.

Viscosity measurements of mineral oil and mixtures of mineral oil with dodecane were required for chapter 4. These were performed by dropping $222 \mu\text{m}$ diameter polystyrene spheres (Duke Scientific, USA) through the oil. The beads slowly sank at a constant rate, since the gravitational force was balanced by a viscous drag force, described by Stokes' law:

$$\frac{4}{3}\pi R^3(\rho_{\text{ps}} - \rho_{\text{mo}})g = 6\pi\eta Rv, \quad (2.1)$$

where $\frac{4}{3}\pi R^3$ is the volume of the sphere, ρ_{ps} and ρ_{mo} are the densities of polystyrene and mineral oil, respectively, g is acceleration due to gravity, v is the sphere's terminal velocity, and η is the mineral oil viscosity. The spheres were allowed to fall for several minutes so that an accurate value of v could be obtained. The particular sphere used for the experiment was not retrieved. Instead, several other spheres were observed and measured under an optical microscope. Spheres had high polydispersity ($CV \approx 12\%$), and so the radius measurement is the largest source of error in calculation of oil viscosity by Eq. 2.1.

2.3 Droplet Clusters

Chapter 5 concerns the compression of 2D droplet clusters between two pipettes and measurement of the corresponding forces from one of the pipettes. Force measurements required resolution of < 100 pN, which is lower than most micropipette deflection measurements [29, 32, 33]. Generally, smaller spring constants correspond to longer pipettes, but the sample chamber dimensions limited the total size of the force-sensing pipette. To accommodate these constraints, long pipettes were bent into compact zig-zag shapes to increase the total length of all segments perpendicular to the applied force, while not extending past the confines of the sample chamber (Fig. 2.1B). To ensure that total compressive force was captured in the deflection of the force-sensing pipette, the pushing pipette was thicker and minimized length of segments that were not parallel to the applied force. Both force-sensing and pushing pipettes were not connected to syringes and were not filled with liquid. The distant ends of the pipette were sealed with mineral oil to prevent suction from capillary forces drawing chamber fluid into the pipettes.

On both types of pipette, the region that contacted the droplets extended ≈ 1 mm from the pipette tip. This region was offset from the rest of the pipette so that it could interact with droplets at the upper surface of the sample chamber while the rest of the pipette could remain near the centre of the chamber (Fig. 2.1A). Pipettes were aligned so that the terminal segment was parallel to the top glass coverslip, with variation of less than one droplet radius over the entire 1 mm length. The two pipettes were also aligned parallel to one another to within ≈ 1 μm variation. To

prevent pipettes touching the upper coverslip, droplet radii had to be larger than pipette radii. However, droplets had to remain small enough that buoyancy did not become important, as this would cause them to move across the field of view if the top coverslip was not completely horizontal at the location of the experiment. Vertically, pipettes were positioned just below the centre of the droplets. This was intended to prevent pipettes sliding above droplets and forcing them out of plane.

If the continuous phase included only water and SDS, droplets experienced a weak attractive interaction. In an effort to increase the strength of this interaction, high molecular weight polyethylene oxide (PEO) was added to the solution to act as a depletant. At high concentrations ($\approx 1\%$), PEO noticeably increased the viscosity of the solution. This was problematic because it resulted in long-range hydrodynamic interactions between moving pipettes and droplets, and also damped the deflection of the force-sensing pipette. At lower concentrations, the interaction strength was increased, but not as much as desired. Instead of adding PEO as a depletant, NaCl was added to the solution as a screening agent. This caused the inter-droplet attractive interaction strength to increase dramatically, with a non-linear dependence on NaCl concentration. A concentration around 2% was found to be ideal for most experiments. After partial evaporation of water, the concentration was estimated to increase as high as 2.1%, which approached the limit for successful experiments. This small change in NaCl concentration resulted in an order of magnitude increase in interaction strength. At higher concentrations, the attractive force between droplets was stronger than the buoyant force. This meant that droplets were not confined to the upper surface of the sample chamber, instead forming tight three-dimensional clusters that could not be easily separated or imaged.

2.4 Image processing and analysis

The experiments described in chapter 3 were performed with a IX271 inverted microscope (Olympus, Japan) and a Retiga 2000R camera (QImaging, Canada). Each frame captured by the camera was saved to the computer's hard drive, at a rate of approximately 1.9 fps. Various magnifications were used. For these experiments, the microscope condenser lens was moved to its highest position, which increased both

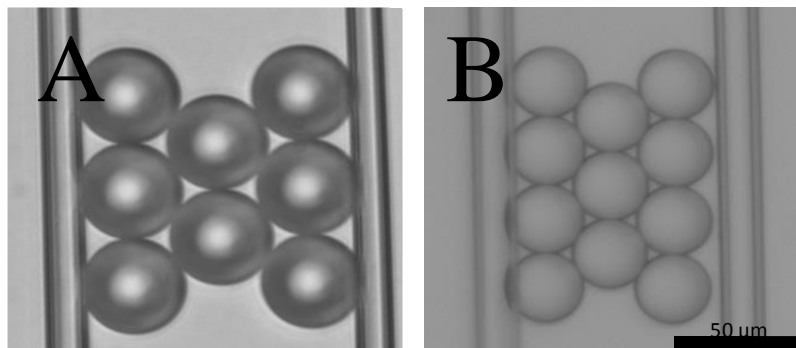


Figure 2.2: Effect of condenser lens position on images. A) Condenser moved to the top of its range. B) Aligned condenser.

the contrast of droplets and the depth of field (Fig. 2.2A). Droplet size was measured from images using the built-in MATLAB `imfindcircles` algorithm. Droplets were tracked across several images, and their size measured in each, to construct a large set of measured radii for each droplet. The mean value for each droplet was then taken to be its actual radius. This approach was necessary to achieve the sub-pixel resolution required to discern size differences between the highly monodisperse droplets. Mean flow rate was calculated for each movie by dividing the total volume of droplets produced by the total time.

The experimental setup was modified slightly for the experiments of chapter 4, dealing with the physical mechanism of droplet snap-off. All images were recorded at the lowest magnification setting of a IX270 inverted microscope (Olympus, Japan) with a Prosilica GT camera (Allied Vision, USA) and StreamPix 5 software (Norpix, Canada). This setup permitted much higher frame rates, up to 60 fps. Due to the `imfindcircles` algorithm's difficulty in identifying extremely large circles, images of large droplets were rescaled so that the droplets did not exceed 100 pixels in diameter. Pipettes were often out of focus in the movies of droplet growth, since they were situated far below the focal plane at the top of the sample chamber. Separate images of each pipette tip were captured for reference purposes.

Compression of droplet clusters, described in chapter 5, required use of the motorized actuator but did not require high frame rates, and so these experiments were performed on the IX271/Retiga 2000R setup used for chapter 3. Both motor advancement and image capture were controlled through a custom Labview script. The

motor was moved at its slowest speed, $0.1 \mu\text{m/s}$. Only every fifth recorded image was saved, resulting in a frame rate of approximately 0.6 fps. For these experiments, it was important to achieve high resolution imaging of droplet edges, and so the microscope condenser lens was aligned (Fig. 2.2B). Positions and radii of droplets were tracked between frames. It was also necessary to determine which droplets were in contact with their neighbours. If the condenser is not aligned, as in Fig. 2.2A, this can be accomplished by comparing image intensity values between the droplet to values within each droplet. Although this should be possible in principle with images taken with an aligned condenser (Fig. 2.2B), it was not implemented. Instead, droplets were considered to be in contact if the distance between their centres was smaller than the sum of the two droplet radii. This method is less robust to changes in illumination or focus across the field of view or throughout the experiment, but is more easily applicable to droplets of multiple sizes. Pipette deflection was measured by comparing intensity values along a line crossing the image of the pipette throughout the movie. Specifically, the position of the pipette was taken as the horizontal shift required to obtain good agreement between a test image and a fixed reference image, as determined through cross-correlation. Sub-pixel resolution was obtained by fitting cross-correlation results to a Gaussian profile to extract a more precise shift value.

Chapter 3

Snap-off production of monodisperse droplets

Solomon Barkley, Eric R. Weeks, and Kari Dalnoki-Veress, *European Physical Journal E* (in press).

This paper was prepared for the new Tips and Tricks section of EPJE, which emphasizes presentation of new scientific methods relevant to soft matter and biological physics. We describe a new technique to produce droplets that are extremely monodisperse. This high monodispersity results from a geometry-dependent instability that causes each droplet to be released at the exact same size. We particularly emphasize the versatility of this technique and its ease of implementation, with a goal that it can be used without extensive expertise or equipment for a variety of applications. Many of the points made in the paper concern specific procedural details that would be useful for other researchers using the technique.

The motivation for this project was primarily to produce droplets for the experiments presented in chapter 5. We needed a droplet-producing method that was reliable and easy to implement without microfluidic components or prior experience. The system that we developed held advantages over other techniques, and so we wanted to make it available to a broader community. I designed and conducted all experiments in consultation with Kari Dalnoki-Veress. I prepared the figures and drafted the manuscript, which was revised by Kari Dalnoki-Veress and Eric R. Weeks.

Snap-off production of monodisperse droplets

Solomon Barkley¹, Eric R. Weeks², and Kari Dalnoki-Veress^{1,3} ^a

¹ Department of Physics & Astronomy and the Brockhouse Institute for Materials Research, McMaster University, Hamilton, ON, Canada

² Department of Physics, Emory University, Atlanta, GA 30322 USA

³ PCT Lab, UMR CNRS 7083 Gulliver, ESPCI ParisTech, PSL Research University, Paris, France

June 23, 2015

Abstract. We introduce a novel technique to produce monodisperse droplets through the snap-off mechanism. The methodology is simple, versatile, and requires no specialized or expensive components. The droplets produced have polydispersity $< 1\%$ and can be as small as $2.5 \mu\text{m}$ radius. A convenient feature is that the droplet size is constant over a 100-fold change in flow rate, while at higher flows the droplet size can be continuously adjusted.

Microfluidics applications often require emulsions with a wide range of characteristics, prompting the development of several distinct techniques for producing droplets [1, 2]. One important parameter is the degree of polydispersity among droplet sizes, where smaller values are preferable for many applications. Droplets with an extremely low polydispersity are particularly desirable for basic science investigations of emulsions [3, 4], vessels for tiny experiments [5–7], as well as calibration in both academic and industrial settings [8]. Here we present a method we have recently developed using glass capillaries and a surface tension driven ‘snap-off’ instability to produce droplets. This method is remarkable for its simplicity, ease of implementation, and the high monodispersity of droplets produced. An additional convenience is that there are two distinct regimes of droplet production: 1) the size of droplets is insensitive at low flow rates; while, 2) at high flow rates the droplet size is tunable.

The snap-off instability of droplets in cylindrically symmetric capillaries was first described in 1970 [9], and has since been investigated further in the context of understanding the physics behind snap-off [10, 11]. We took advantage of this effect to develop a versatile system for production of monodisperse droplets that is easy to assemble and operate. One important consideration is that this setup requires no flow of the continuous phase, since the pinch-off is driven by surface tension forces rather than viscous forces. Although the snap-off process has been used previously to produce droplets in flattened microfluidic geometries [12–14], our simple cylindrical configuration is able to produce droplets that are more monodisperse.

In order to prepare monodisperse droplets we have utilised a method that is schematically depicted in Fig. 1.

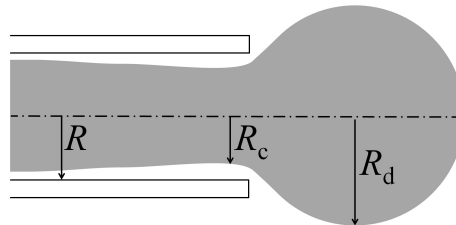


Fig. 1. Schematic of the experimental setup before a droplet snaps off. A column of dispersed phase (grey) with minimum radius R_c is ejected from a glass capillary with inside radius R into the dispersed phase (white). The continuous phase forms a thin wetting layer along the inside of the tube. The dispersed phase forms a growing droplet of radius R_d at the end of the tube.

A thin glass capillary tube of radius R is filled with the dispersed phase which is ejected with some flow rate into the continuous phase. A growing droplet forms at the end of the tube with radius R_d . At low flow rates we can treat the system as being quasi-static. This dictates that the dispersed phase immediately inside the tube has the same pressure as that in the droplet [9, 13]. However, due to Laplace pressure, the pressure of the continuous phase surrounding the dispersed phase is not uniform and varies with axial position. The Laplace pressure decrease between the dispersed phase and continuous phase is $\Delta P_d = 2\gamma/R_d$ for the droplet, with interfacial tension γ [15]. If the continuous phase wets the capillary, then a thin wetting layer coats the inside surface of the tube. We define the collar to be the point at which the radius of the dispersed phase within the tube is a minimum, $R_c \leq R$. Since the radius at the collar is much smaller than the orthogonal radius, we can neglect the orthogonal contri-

^a email: dalnoki@mcmaster.ca

tribution to the Laplace pressure at the collar and write the Laplace pressure decrease at the collar as $\Delta P_c = \gamma/R_c$. Using the fact that the pressure in the dispersed phase is the same at the collar and in the droplet, the pressure difference between the continuous phase at the collar and that in the bulk is given by the difference in these two Laplace pressures:

$$\Delta P = \Delta P_d - \Delta P_c = \gamma \left(\frac{2}{R_d} - \frac{1}{R_c} \right). \quad (1)$$

It follows that if $\Delta P < 0$, the continuous phase will be drawn into the tube around the dispersed phase and the wetting layer thickens (R_c decreases and thus ΔP becomes more negative). Conversely the continuous phase will be ejected from the tube if $\Delta P > 0$.

To illustrate the formation of the droplets we show a sequence of optical microscopy images of the snap-off process in Fig. 2. Initially, the dispersed phase is contained entirely within the tube (Fig. 2a) and the wetting layer of the continuous phase is very thin along the entire length of the tube ($R_c \sim R$). Upon ejection, the dispersed phase forms a very small droplet (Fig. 2b). At this point the Laplace pressure in the droplet, ΔP_d , is high relative to that within the tube due to the high curvature of the small droplet. Thus there exists a positive pressure difference ΔP of the continuous phase between the inside and outside of the tube (see Eq. 1). As the droplet grows (Fig. 2c), both ΔP_d and ΔP decrease as a result of increasing R_d , until $\Delta P_d < \Delta P_c$, or equivalently $\Delta P < 0$. Once $\Delta P < 0$ the continuous phase begins to invade the tube (visible as darkening in Fig. 2d): the configuration is unstable and there is a spontaneous reverse flow of the continuous phase. The continuous phase forms a collar around the dispersed phase which is marked by an arrow in Fig. 2e. During this phase R_c and ΔP decrease rapidly causing the collar to collapse – the ‘snap-off’ of the droplet is complete and the process repeats (Fig. 2f).

In the experiments presented the tube was a thin glass pipette. Pipettes were prepared using a pipette puller (Narishige, Japan) from glass capillaries (World Precision Instruments, USA) with initial outside diameter 1 mm and inside diameter 580 μm . The pipettes used had an outside diameter ranging from $< 3 - 1000 \mu\text{m}$. We note that we have also prepared a similar device simply by heating a capillary tube over an ethanol flame and stretching it manually – a pipette puller is merely a convenience. Unless otherwise specified the continuous phase is water and the dispersed phase is mineral oil. Droplets were stabilized against coalescence by adding surfactant (1% sodium dodecyl sulphate) to the continuous water phase. Mineral oil was forced out of the pipette by applying pressure to a syringe connected to the pipette, or by adjusting the height of an oil reservoir. As discussed, to facilitate the snap-off process there has to be a thin layer of the continuous phase surrounding the dispersed phase inside the pipette. Wetting of the inside surface of the pipette by the continuous phase was achieved by briefly reversing flow in the tube before droplet production.

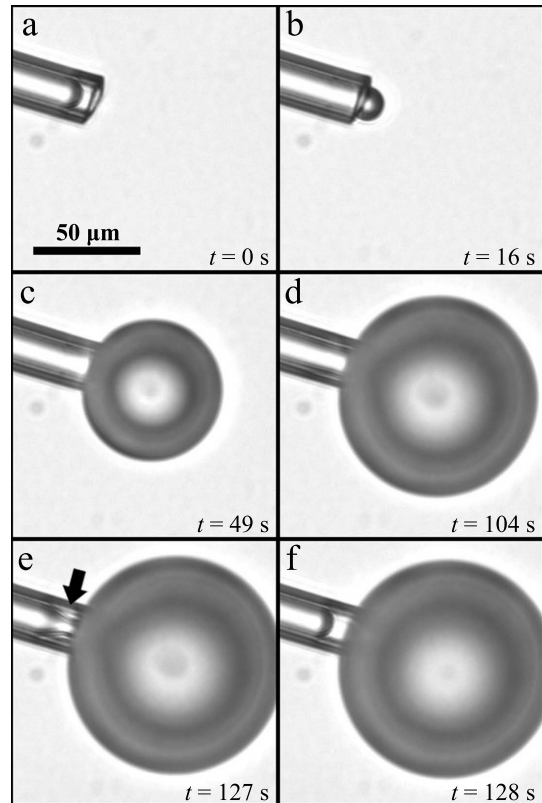


Fig. 2. Time series of a droplet growing until snap-off. a-c) Mineral oil is ejected from the tip of a glass pipette into water, forming a growing droplet. d) Water is spontaneously drawn into the end of the pipette once the droplet has reached a critical size. e) The water forms a collar around the column of oil flowing outwards. f) The collar constricts and snaps off the droplet. We note that the timescales over which the images were taken in this sequence is much longer than typical. The slow rate was required in order to image the rapidly forming collar structure.

For certain applications, it may be desirable to produce water droplets in oil. This was achieved by coating the pipette with polystyrene which is wet by mineral oil as opposed to water. A solution was prepared by dissolving polystyrene of molecular weight $M_w = 8.8 \text{ kg/mol}$ in toluene at a concentration of 20% (Polymer Source, Canada). A pipette was then coated by dipping its tip into the polystyrene solution and expelling air through the pipette as the solvent evaporated. Indeed, the crucial aspect is the wettability of the inside surface of the pipette by the continuous phase – given that constraint the snap-off phenomenon can be made to occur for a wide range of liquids [11, 13].

Snap-off droplet size is influenced by both the diameter of the pipette and the shape of the pipette tip. By changing the radius R of the pipette used to produce the droplets, it is possible to vary the radius R_d of droplets from 2.5 – 750 μm . For snap-off to occur, the continuous phase must enter the tip of the pipette as the droplet

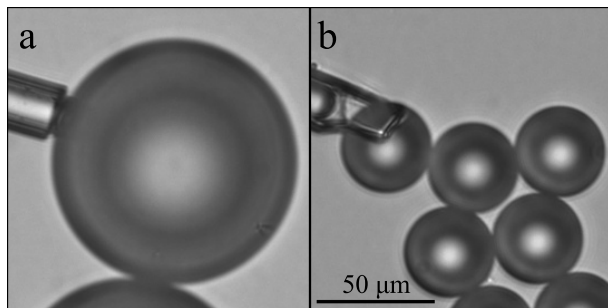


Fig. 3. Effect of pipette tip shape on snap-off droplet production. a) A tip that has a flat opening produces large droplets. b) After the tip of the pipette shown in (a) is broken irregularly, it produces droplets that are smaller and more monodisperse.

is produced. If the pipette has a completely flat tip, as in Fig. 2, the circular opening is occluded by the growing spherical droplet. As a result, the continuous phase is unable to easily flow into the pipette and snap-off is delayed. To illustrate the effect of tip shape, a pipette that initially had a flat tip geometry is shown in Fig. 3a. That tip was then broken off with a pair of tweezers to produce the irregular tip shown in Fig. 3b, and the same pipette produces droplets that are both smaller and more monodisperse when it has an irregular tip shape. The irregularity of the tip facilitates the reverse flow of the continuous phase into the pipette. Eq. 1 predicts snap-off in the quasi static regime when $\Delta P < 0$, or alternatively, when $R_d > 2R$. This condition applies only for irregular tips where the flow of the continuous phase into the pipette is unimpeded. The importance of an irregular opening for snap-off has been demonstrated previously in a different geometry [9].

Despite the variation in droplet size between pipettes, there is very little variation in the size of droplets produced from the same pipette at a given flow rate. A standard measure of monodispersity is the coefficient of variation (CV) in droplet radius, defined as the standard deviation in droplet radii normalized by the mean droplet radius. Pipettes with irregular tips, which are both easy to prepare and most ideal for droplet production, like that shown in Fig. 3b, produce droplets with radius CV of 0.5%. These droplets are more monodisperse than those produced through other recently developed methods, which all report polydispersity $> 1\%$ [7,12–14,16–20]. It should be noted that our measurement of droplet radius CV is limited by the precision with which we are able to measure individual droplet radii (~ 60 nm), and so the quoted value represents an upper bound on the actual radius CV.

The quasi-static approximation is valid only in the limit of negligible flow of the dispersed phase from the end of the pipette (i.e. when the pressure gradient driving the flow is negligible compared to those in Eq. 1). At higher flow rates, snap-off droplets are found to be larger than would be predicted by Eq. 1. The size of droplets produced by snap-off from a single pipette R_d is shown as a function of volumetric flow rate Q in Fig. 4. For $Q < 50$ pL/s,

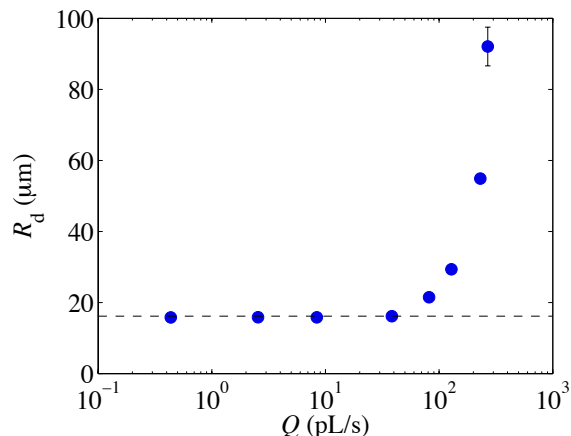


Fig. 4. Effect of volumetric flow rate Q on droplet radius R_d for snap-off droplets produced from the same pipette. The horizontal dashed line is the quasi-static prediction from pipette diameter, $R_d = 2R$. Other than the error bar shown for the highest flow rate (mean \pm standard deviation), the error in the droplet size was much smaller than the data points due to the droplets' monodispersity.

droplet size is constant, and is in excellent agreement with $R_d = 2R$, as predicted by Eq. 1 and shown in Fig. 4 as the black horizontal dashed line. The quasi-static approximation is valid over a 100-fold increase in flow rate, with no measurable change in R_d up to 50 pL/s. The insensitivity of droplet size to flow rate in this regime provides a simple approach to produce monodisperse droplets even with poor control over pressure or flow rate of the dispersed phase (i.e applying pressure to a syringe by hand). Additionally, we find that the droplet production rate can be adjusted continuously through control of flow rates in the quasi-static regime, to a maximum of ~ 2 droplets per second for the type of data shown in Fig. 4. The production rate represents one of the disadvantages of the snap-off process described here – oftentimes higher rates of production are desirable.

As can be seen in Fig. 4, with large flow rates the droplet size increases monotonically. The high flux of the dispersed phase out of the pipette prevents the reverse flow of the continuous phase, and snap-off is delayed – the quasi-static assumption is no longer valid. An added convenience of the snap-off methodology is that in this regime, droplet size is tunable by adjusting the flow rate without a need to change the radius of a pipette. In Fig. 4 the size of the droplets is increased by a factor of ~ 5 over a ~ 10 -fold increase in flow rate with no adverse effects to droplet monodispersity. (We note that at the highest flow rate the error bar does reflect an adverse scatter in the droplet radii, and attribute this to a lack of fine control in achieving a constant flow rate at that value). The five-fold increase in droplet size is not a fundamental limitation, rather if the flow rate is increased even further, snap-off ceases entirely, and the droplet grows indefinitely [11].

In conclusion, snap-off droplet generation in pre-wet cylindrical glass capillaries is advantageous for its simplicity, versatility, and the monodispersity of produced droplets. All of the system components are readily available and no specific technical expertise is required. Droplet size can be altered by replacing the pipette or by increasing the volumetric flow rate of the dispersed phase, which can be either water or oil. A quasi-static description successfully predicts a constant droplet size over a wide range of flow rates below some critical value. The main distinction between our technique and the majority of prior techniques is that our outer fluid (the continuous phase) is not flowing, so the constriction and subsequent pinch-off of the dispersed phase is due to surface tension forces imposed by the shape of the glass capillary rather than viscous forces.

Financial Support for this work was provided by National Sciences and Engineering Research Council (NSERC). The work of E.R.W. was supported by the National Science Foundation under Grant No. CBET-1336401.

References

1. G.F. Christopher, S.L. Anna, *J. Phys. D: Applied Physics* **40**(19), R319 (2007)
2. R. Seemann, M. Brinkmann, T. Pfohl, S. Herminghaus, *Rep. Prog. Phys.* **75**(1), 016601 (2012)
3. J.C. Baret, F. Kleinschmidt, A. El Harrak, A.D. Griffiths, *Langmuir* **25**(11), 6088 (2009)
4. K.W. Desmond, P.J. Young, D. Chen, E.R. Weeks, *Soft Matter* **9**(12), 3424 (2013)
5. C.A. Stan, G.F. Schneider, S.S. Shevkoplyas, M. Hashimoto, M. Ibanescu, B.J. Wiley, G.M. Whitesides, *Lab Chip* **9**(16), 2293 (2009)
6. S. Selimovic, F. Gobeaux, S. Fraden, *Lab Chip* **10**(13), 1696 (2010)
7. H. Tanaka, S. Yamamoto, A. Nakamura, Y. Nakashoji, N. Okura, N. Nakamoto, K. Tsukagoshi, M. Hashimoto, *Anal. Chem.* **87**(8), 4134 (2015)
8. H. Ulmke, T. Wriedt, K. Bauckhage, *Chemical Engineering and Technology* **24**(3), 265 (2001), ISSN 1521-4125
9. J. Roof, *Society of Petroleum Engineers Journal* **10**, 85 (1970)
10. R. Lenormand, C. Zarcone, A. Sarr, *Journal of Fluid Mechanics* **135**, 337 (1983)
11. T. Peña, M. Carvalho, V. Alvarado, *AIChE journal* **55**(8), 1993 (2009)
12. R. Dangla, S.C. Kayi, C.N. Baroud, *Proc. Nat. Acad. Sci.* **110**(3), 853 (2013)
13. K. van Dijke, R. de Ruiter, K. Schroën, R. Boom, *Soft Matter* **6**(2), 321 (2010)
14. F. Malloggi, N. Pannacci, R. Attia, F. Monti, P. Mary, H. Willaime, P. Tabeling, B. Cabane, P. Poncet, *Langmuir* **26**(4), 2369 (2010)
15. P.G. de Gennes, F. Brochard-Wyart, D. Quéré, *Capillarity and Wetting Phenomena: Drops, Bubbles, Pearls, Waves* (Springer, New York, 2003)
16. W.A.C. Bauer, J. Kotar, P. Cicuta, R.T. Woodward, J.V. Weaver, W.T. Huck, *Soft Matter* **7**(9), 4214 (2011)
17. H. Duan, W. Yang, C. Li, B. Lojewski, W. Deng, *Aerosol Science and Technology* **47**(11), 1174 (2013)
18. M.K. Mulligan, J.P. Rothstein, *Microfluidics and nanofluidics* **13**(1), 65 (2012)
19. C. Priest, S. Herminghaus, R. Seemann, *Applied physics letters* **88**(2), 024106 (2006)
20. V. Chokkalingam, B. Weidenhof, M. Krämer, W.F. Maier, S. Herminghaus, R. Seemann, *Lab on a Chip* **10**(13), 1700 (2010)

Chapter 4

Predicting the size of droplets produced through Laplace pressure induced snap-off

Solomon Barkley, Samantha J. Scarfe, Eric R. Weeks, and Kari Dalnoki-Veress, to be submitted to Soft Matter

In this work, we explored the impact of changing several system parameters on the size of droplets produced through the snap-off technique. We introduced and tested a model to describe the stability of a growing droplet and the point at which it snaps-off in terms of simple balancing of pressures. Our model predicted unexpectedly rich criteria for droplet stability that we verified experimentally. We examined the impact of changing geometry and fluid properties on droplet sizes produced at different flow rates, and found some contradictions with assumptions of previous studies.

During development of the snap-off technique, we sought an understanding of the underlying physical mechanism. However, this information was not compatible with the goals of the tips and tricks article, and required different experiments. I conceived and designed the experiments, which were conducted by Samantha Scarfe in consultation with myself and Kari Dalnoki-Veress. Both Samantha Scarfe and I performed data analysis using MATLAB scripts that I wrote. I prepared figures and drafted the manuscript, subject to revision by Kari Dalnoki-Veress and Eric Weeks.

Cite this: DOI: 10.1039/xxxxxxxxxx

Predicting the size of droplets produced through Laplace pressure induced snap-off

Solomon Barkley,^a Samantha J. Scarfe,^a Eric R. Weeks,^b and Kari Dalnok-Veress^{*ac}

Received Date
Accepted Date

DOI: 10.1039/xxxxxxxxxx

www.rsc.org/journalname

Laplace-pressure driven snap-off is a technique that is widely used to produce droplets for emulsions and microfluidics purposes. Previous predictions of droplet size have assumed a quasi-equilibrium low flow limit. We present a simple model to predict droplet sizes over a wide range of flow rates, demonstrating a rich landscape of droplet stability depending on droplet size and growth rate. The model is able to account for the frequently adjusted experimental parameters of geometry, interfacial tension, and the viscosities of both phases.

1 Introduction

With the development of numerous techniques to produce micron-scale droplets, there has been a growing interest in exploring the physical mechanisms behind these methods^{1–5}. A greater understanding of which parameters are most important to droplet production can permit fine-tuning of techniques or modification of systems where droplet production is undesirable^{6–8}. Laplace pressure driven snap-off relies upon an instability that forms when a confined dispersed phase is allowed to penetrate into a larger space filled with an immiscible continuous phase. The instability requires no viscous interaction, but is due entirely to changes in the curvature of the interface between the two phases, affecting the Laplace pressure. We have previously found that the resulting droplets are highly monodisperse⁹, as the system becomes unstable immediately after the protrusion of the dispersed phase reaches a critical size. The snap-off phenomenon has been studied and used to produce droplets in many different geometries^{4,5,8–10}. However, the case of ejecting the dispersed phase from a cylindrically symmetric tube is the simplest from a theoretical standpoint^{6,9,11}.

By neglecting pressure gradients within the dispersed phase, several groups have been able to provide a theoretical framework for droplet sizes in a quasi-static regime^{5,8,9,11}. The approximation of a static dispersed phase has been shown to be valid in regimes that are useful for droplet production^{2,5,9}. Additionally, it was shown that droplets grow larger before snapping off at higher flow rates, and eventually grow indefinitely for sufficiently large flow rates^{6,8,9,12}. The ability to deliberately vary droplet size without changing the apparatus, for instance by changing

the flow rate, represents a valuable experimental tool. Nevertheless, a model which can predict the size of snap-off droplets at flow rates where the quasi-static approximation is no longer valid has remained elusive. Previous studies have examined the effects of changes in geometry, interfacial tension, and viscosity ratio between the two fluids on the droplet production^{2,5–8,12}. However, many of these investigations have been largely qualitative in nature.

Here, we present experiments that are compared to a model predicting the size of droplets produced through the snap-off mechanism over a wide range of flow rates. The model provides a “stability diagram”: regions on a plot of the droplet radius as a function of the flow rate where droplets are stable and grow and regions where the droplets become unstable and snap off. The stability diagram enables manipulation of the system to produce droplets at both sizes and flow rates where snap-off would not normally occur. Furthermore, the model we present accounts for the effects of fluid properties and geometry on the droplet production. The work presented is carried out in the cylindrically symmetric geometry, although the ideas are easily extended to the flattened geometries that are common for snap-off droplet production.

2 Theory

Snap-off occurs when a dispersed phase is ejected from a nozzle into a reservoir of a continuous phase as shown in Fig. 1. The dispersed phase forms a growing spherical droplet that becomes unstable at some critical size and subsequently snaps-off⁹. Assuming a quasi-equilibrium, we can define the pressure of the bulk continuous phase P_0 , and an increased pressure in the droplet of dispersed phase P_d due to the droplet's Laplace pressure $P_d = P_0 + 2\gamma/R_d$, where R_d is the radius of the droplet and γ is the interfacial tension between the dispersed and continuous phase. In more complex, non-cylindrical geometries, growth of

^a Department of Physics and Astronomy, McMaster University, Hamilton, ON, Canada. E-mail: dalnoki@mcmaster.ca

^b Department of Physics, Emory University, Atlanta, GA 30322 USA.

^c PCT Lab, UMR CNRS 7083 Gulliver, ESPCI ParisTech, PSL Research University, Paris, France.

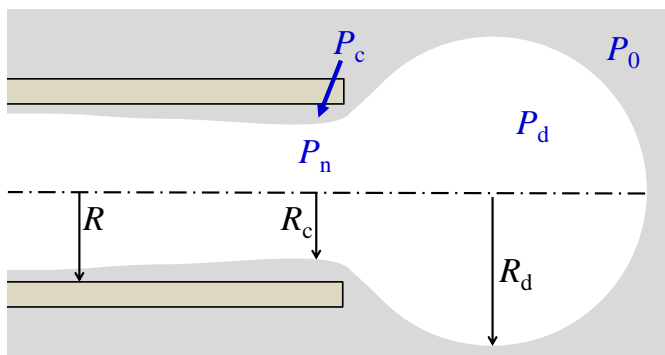


Fig. 1 Schematic illustrating the important dimensions and pressures in the system. The inner radius of the cylindrical nozzle R , minimum radius of the flowing dispersed phase column within the nozzle R_c , and radius of the growing droplet R_d define the relevant length scales. The relevant pressures are the pressure of the bulk continuous phase P_0 , pressure of the dispersed phase in the growing droplet P_d , pressure of the dispersed phase in the nozzle P_n , and the pressure of the continuous phase in the collar around the dispersed phase P_c . Snap-off occurs when the continuous phase flows from the bulk into the collar, thereby decreasing R_c to the point of snap-off ($P_c < P_0$).

the droplet is restricted in one or more directions, and the Laplace pressure difference will depend on the dimensions of the confining chamber^{5,8,11}. For snap-off to proceed effectively, there must be a wetting layer of the continuous phase coating the interior of the nozzle containing the dispersed phase, which forms a transient collar – a minimum radius in the dispersed phase, R_c ^{9,11}. Again, due to the curvature of the interface at the collar, we can write the Laplace pressure difference between the dispersed phase in the nozzle P_n and the continuous phase in the surrounding collar P_c ,

$$P_n = P_c + \frac{\gamma}{R_c}. \quad (1)$$

Here we have made two simplifying assumptions which are consistent with experimental observations: 1) in the case of a cylindrical nozzle, the radius of the collar R_c is approximately equal to the nozzle radius R , since the wetting layer of the continuous phase is thin; and 2) R_c is a much smaller radius than that of the orthogonal curvature.

The snap-off instability develops when $P_c < P_0$, causing a reverse flow of the continuous phase from the bulk P_0 into the collar P_c . As the continuous phase flows, the collar constricts the dispersed phase (R_c decreases), which reduces P_c relative to P_n according to Eq. 1. This exacerbates the pressure difference driving reverse flow of the continuous phase, and the collar structure rapidly collapses, releasing the droplet^{2,9}. Previous efforts to predict snap-off droplet size have been restricted to the low flow limit of the dispersed phase^{2,5,9,11}. In this case, $P_d = P_n$ and the snap-off condition can be written as

$$P_0 + \frac{2\gamma}{R_d} - \frac{\gamma}{R} = P_0 \quad (2)$$

for the case of a cylindrical nozzle and a droplet that is free to grow in all directions. Eq. 2 can be simplified to predict $R_d = 2R$ in the low-flow limit as we have shown in a previous study⁹. At higher flow rates, there will be a pressure gradient along the

cylindrical nozzle described by Poiseuille flow¹³,

$$\frac{dP}{dx} = \frac{8\eta Q}{\pi R^4}, \quad (3)$$

where η is the viscosity of the dispersed phase and Q is the volumetric flow rate. We are concerned with the pressure difference between the dispersed phase at the collar, P_n , and that in the droplet, P_d . In practice, nozzles with circular apertures are undesirable, as spherical droplets block the opening and prevent the reverse flow of the continuous phase that is necessary for snap-off to occur^{9,11}. Cylindrical nozzles must therefore have an irregular tip shape that is not easily controlled between nozzles. The drop in pressure from P_n to P_d occurs over a length scale with two distinct components. First, each tip contributes a geometric parameter L that is specific to the pipette tip's unique shape. Second, the pressure must drop to P_d by some distance into the droplet, which contributes εR_d , since this dimension scales with the droplet radius. By inserting L and εR_d into Eq. 3, we obtain

$$P_n = P_d + \frac{8\eta Q}{\pi R^4} (L + \varepsilon R_d). \quad (4)$$

We have now established relationships between each of the pressures depicted in Fig. 1, allowing us to rewrite the snap-off condition for increasing flow rates. By combining Eqs. 2 and 4 we obtain,

$$P_0 + \frac{2\gamma}{R_d} + \frac{8\eta Q}{\pi R^4} (L + \varepsilon R_d) - \frac{\gamma}{R} = P_0. \quad (5)$$

Introducing the non-dimensional variables $\tilde{R}_d = \frac{R_d}{R}$, $\tilde{L} = \frac{L}{R}$, and $\tilde{Q} = \frac{8\eta Q}{\pi\gamma R^2}$, Eq. 5 can be rearranged to

$$0 = \varepsilon \tilde{Q} \tilde{R}_d^2 + (\tilde{L} \tilde{Q} - 1) \tilde{R}_d + 2. \quad (6)$$

Finally, Eq. 6 can be solved for \tilde{R}_d as a function of \tilde{Q} :

$$\tilde{R}_d = \frac{1 - \tilde{L} \tilde{Q} \pm \sqrt{(1 - \tilde{L} \tilde{Q})^2 - 8\varepsilon \tilde{Q}}}{2\varepsilon \tilde{Q}}. \quad (7)$$

Eq. 7 defines a critical non-dimensional droplet radius \tilde{R}_d for a given rescaled flow rate \tilde{Q} . Beyond the critical radius, the continuous phase invades the nozzle containing the dispersed phase, causing the droplet to snap-off. Eq. 7 can thus be interpreted as follows. For a given flow rate, the droplet grows, while still attached by the collar to the dispersed phase. Eventually the droplet grows to the critical radius given by Eq. 7 at which point the collar pinches off and the droplet is released into the continuous medium. Eq. 7 thus defines the boundary between stable and unstable droplets in a parameter space of \tilde{R}_d and \tilde{Q} as shown by the lower solid line in Fig. 2.

The above explanation assumes that the negative square root is taken in Eq. 7. If the positive square root is taken instead, Eq. 7 defines a minimum stable droplet size as a function of flow rate, shown as the dashed line in Fig. 2. Droplets larger than this critical size are stable to continue growing indefinitely as the $\varepsilon \tilde{Q} \tilde{R}_d^2$ term dominates Eq. 6.

In reality, no droplets are able to grow indefinitely, as large droplets break away from the pipette due to their buoyancy. It

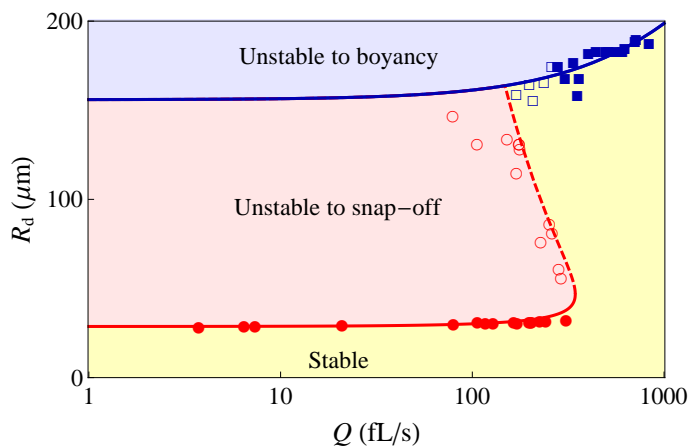


Fig. 2 Stability diagram for droplets as they grow at a particular flow rate from a single pipette. Droplets growing at a constant flow rate break away from the pipette either upon snap-off (solid circles) or due to buoyancy (solid squares), when they cross the stability lines of either phenomenon given by the solid lines (Eqs. 7 and 8, respectively). Droplets produced with a flow rate that is not constant and decreasing can be made to snap-off at intermediate sizes (open symbols) after crossing the dashed line (Eq. 7).

is important to note that this separation represents a different mechanism than the Laplace-pressure driven snap-off. The size at which buoyant forces are sufficient to separate the droplet from the pipette depends on both the shape and orientation of the tip, as well as the flow rate. We assume that for a particular pipette, there is some critical droplet volume V_b beyond which the droplet is unstable to buoyancy. However, droplets take some fixed amount of time τ to detach from the pipette and continue to grow at the same flow rate during this time. The volume of droplets that break away from the pipette is therefore expressed simply as $V_d = V_b + Q\tau$. Droplet radius at buoyant separation is given by:

$$R_d = \frac{3\pi}{4} (V_b + Q\tau)^{\frac{1}{3}}, \quad (8)$$

which is plotted as the upper solid curve in Fig. 2.

3 Experiment

Cylindrical nozzles were created by stretching capillary tubes (World Precision Instruments, USA) with a pipette puller (Narishige, Japan). Initial capillary inner diameter was $540 \mu\text{m}$ and final pipette inner diameter was on the order of $\approx 10 \mu\text{m}$. Pipette ends were clipped with tweezers after stretching to produce a jagged tip shape unique to each pipette. As discussed above (see also⁹), jagged pipettes were found to perform optimally in comparison to perfectly flat ends that allow the droplet to seal the tip, thus preventing the reverse flow that results in snap-off. In fact, the pipettes are not perfectly cylindrical, but taper gradually from diameter $\approx 100 \mu\text{m}$ to $\approx 10 \mu\text{m}$ over several centimetres, and so pipettes with larger openings can be produced by breaking the pipettes further from the tip. Unless otherwise stated, the dispersed phase was mineral oil and the continuous phase was water with 1% (by weight) sodium dodecyl sulphate (SDS) added to stabilize droplets against fusion. Droplets were produced by

ejecting oil out of a pipette into a chamber of the water phase, taking care that the pipette tip was far from any chamber boundaries. The flow rate was controlled by maintaining a connected oil reservoir at a constant pressure, either by adjusting its height or by clamping a syringe. This procedure resulted in a constant flow rate at the pipette tip as long as the volume of oil leaving the pipette is negligible compared to the oil reservoir. Droplets were imaged from below at up to 50 frames per second.

Viscosity of the oil phase was decreased for some experiments by mixing dodecane with the mineral oil in concentrations up to 50% by weight. Viscosity of the water phase was increased for some experiments by adding glycerol at concentrations up to 60%, with the SDS concentration maintained at 1%. Interfacial tension between the two phases was increased for some experiments by reducing the concentration of SDS in the water phase, to a minimum of 0.05%. Viscosity of mineral oil was measured by allowing a $225 \mu\text{m}$ diameter polystyrene bead (Duke Scientific, USA) to slowly fall through a column of oil. A high precision measurement of its terminal velocity was used to calculate viscosity through Stokes' law. This experiment was repeated with the mineral oil-dodecane mixtures, and its results compared to the predictions of ASTM blending method to calculate viscosity¹⁴.

For certain experiments, it was necessary to reduce the oil flow rate during droplet growth. By doing so, the trajectory of a droplet's growth is not simply a vertical line in the stability diagram. To accomplish this, the oil reservoir was slowly lowered once the droplet had grown to an intermediate size. The oil reservoir was fixed at its new height upon snap-off of the growing droplet. For droplets growing at a constant flow rate, total droplet volume released in a timed experiment was used to determine the flow rate. In order to measure the flow rate at snap-off for droplets growing at a decreasing flow rate, a number of additional droplets were allowed to form after fixing the reservoir height, and the flow rate of these droplets was measured. This method can only provide a lower bound for the flow rate of the droplet produced at decreasing flow rate.

4 Results & Discussion

For a given pipette, droplets can be produced at many different flow rates. At low flow rates, droplet size is independent of flow rate over orders of magnitude changes to Q , as predicted by Eq. 2 (solid circles in Fig. 2). At higher flow rates, droplet size at snap-off increases with flow rate, until the flow rate reaches some critical value (Fig. 3). This observation of a critical value agrees well with previous results^{9,12}. For sufficiently large \tilde{Q} , there is no droplet size \tilde{R}_d that can satisfy Eq. 6 and droplets would be expected to grow indefinitely^{6,9}. In practice, droplets produced beyond the critical flow rate eventually break away from the pipette due to their buoyancy (solid squares in Fig. 2). Droplet radius at the time of separation due to buoyancy is described by Eq. 8 and is plotted as the upper curve in Fig. 2, which is a fit to the square data points and returns a critical droplet volume $V_b = 1.6 \text{ pL}$ and a detachment time $\tau = 1.7 \text{ s}$.

Droplets growing at a constant flow rate can be interpreted as an upwards vertical trajectory in the stable region of Fig. 2. Droplets will break away from the pipette either upon snap-off at

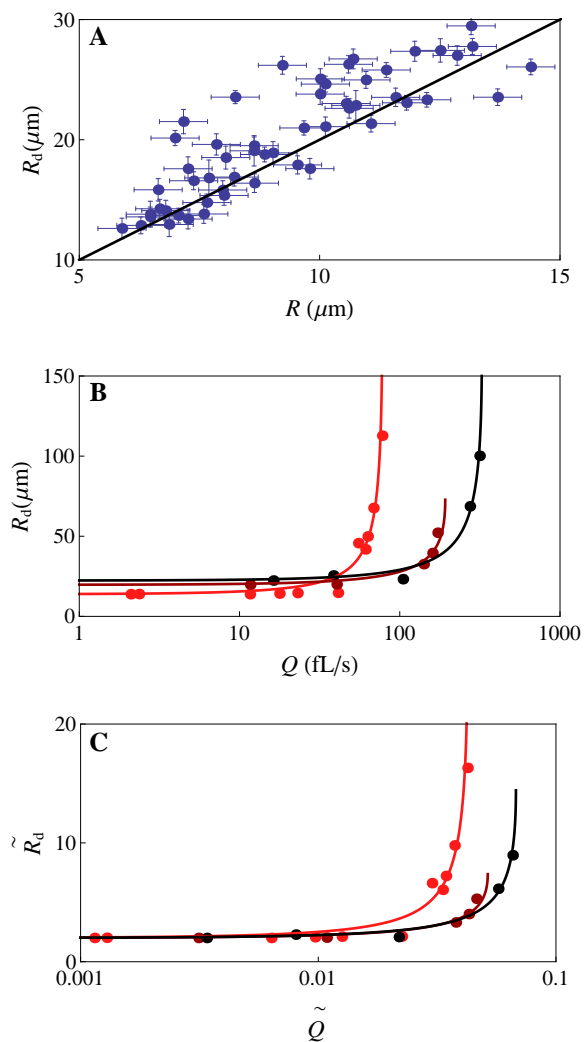


Fig. 3 Effect of pipette dimensions on droplet radius. A) Minimum observed radius of droplets for many different pipette radii, showing good agreement with prediction for the low-flow limit (black line). B) Snap-off droplet size for increasing flow rate through three different pipettes. Curves are fits to Eq. 7. C) Same data as in B), but with scaled droplet radius and flow rate.

low flow rates (solid circles in Fig. 2), or due to buoyancy at high flow rates (solid squares). For many pipettes, the droplets produced through these two mechanisms have very different sizes and it is not possible to produce droplets of intermediate size at any constant flow rate. The snap-off droplets produced for different constant flow rates agree with the prediction of Eq. 7 if the negative square root is taken (lower solid curve in Fig. 2, with $\tilde{L} = -4.5$ and $\varepsilon = 3.7$).

Since droplets grow (i.e. R_d increases for positive Q), it is only possible to travel upwards in the R_d - Q stability diagram. The inverted large-droplet branch of the snap-off curve is not normally accessible, as it would require passing from an unstable droplet (which cannot remain attached to the pipette) to a stable one. However, individual droplets can be produced at continuously decreasing flow rates, represented as a diagonal trajectory towards the upper left in Fig. 2. When these droplets fulfil an alternate (root) solution to the snap-off condition Eq. 7, they cross

the dashed portion of the snap-off stability curve in Fig. 2 from right to left. This causes the droplets to become unstable and they subsequently snap-off, represented by the open circles in Fig. 2. As it is not possible to measure the instantaneous flow rate of these droplets, the flow rate of smaller droplets produced immediately afterwards at the same, fixed flow rate is measured instead. Because these subsequent droplets may have actually been produced at a slightly lower flow rate, the flow rate thus obtained provides an underestimate for the flow rate at snap-off of the earlier droplet.

Snap-off of droplets at decreasing flow rates provides a mechanism to produce intermediate sized droplets that are not normally accessible with a particular pipette. However, only individual droplets can be produced in this manner. While there is little value of this approach to droplet production, such experiments provided an excellent verification of the model. The presence of this typically inaccessible branch of the snap-off curve confirms that at intermediate flow rates, both small and large droplets are permitted to grow but medium droplets are unstable to snap-off. The stable portion of the R_d - Q diagram corresponding to large droplets is not accessible at a constant flow rate, since this would require droplets to pass through the unstable intermediate sizes (intermediate region in Fig. 2).

One of the most straightforward methods to produce snap-off droplets of a different size is to alter the chamber dimensions^{2,8,9,12}. In the case of a cylindrical nozzle ejecting a dispersed phase into an unconfined bulk continuous phase, the only dimension in the system is the radius of the nozzle, R . In the low flow limit, Eq. 2 predicts droplet size $R_d = 2R$ or $\tilde{R}_d = 2$ (see also reference⁹). This prediction is confirmed by Fig. 3A, which plots the minimum droplet size observed at low flow rates against inner pipette radius for many pipettes, along with the prediction from Eq. 2 (black line). Due to the difficulty in accurately measuring the pipette inner radius R , we assume it can be approximated as half the radius of the smallest droplet size from a given pipette for the remainder of this study. At higher flow rates, the dependence of \tilde{R}_d on R is non-trivial, as both \tilde{L} and \tilde{Q} in Eq. 7 are normalized by R and R^2 , respectively. Fig. 3B shows data from three separate pipettes with different radii. For each pipette, the characteristic curve of droplet radius R_d is plotted as a function of volumetric flow rate Q . The same data is plotted in terms of scaled variables \tilde{R}_d and \tilde{Q} in Fig. 3C demonstrating good collapse in the vertical direction (collapse is not expected in the horizontal direction, even if pipettes shared values of \tilde{L} and ε). All datasets were fit to Eq. 7, with oil viscosity measured as $\eta = 123 \pm 4$ mPa.s and interfacial tension taken as $\gamma = 12$ mN/m based on related literature^{7,15,16}. Both \tilde{L} and ε are expected to depend on the precise tip shape, and are expected to vary between pipettes. Nevertheless, we find $l \approx 10$ and $\varepsilon \approx 0.1$, both of which are reasonable.

The snap-off process is driven by the interfacial tension between the two phases. However, the actual value of γ does not affect droplet production in the low flow limit, since it is present in each term of Eq. 2 (this was also observed in reference⁷). At higher flow rates, interfacial tension influences the non-dimensionalized flow rate $\tilde{Q} \propto Q/\gamma$. The interfacial tension between mineral oil and water is large ($\gamma = 48$ mN/m), and is

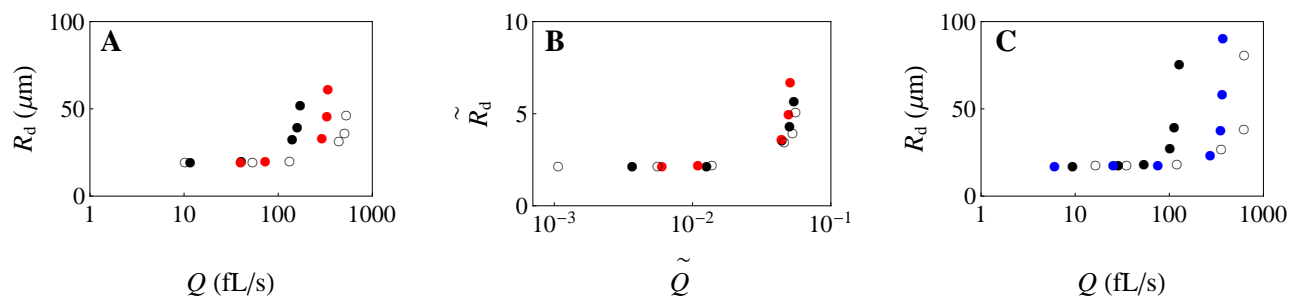


Fig. 4 A) Droplets sizes produced from a single pipette at increasing flow rates for SDS concentrations of 1% (black circles), 0.01% (lighter filled circles), and 0.005 % (open circles). B) Same data as in A) plotted in terms of non-dimensional units. C) Droplet sizes produced from a single pipette at increasing flow rates for oil viscosities of 123 mPa.s (black circles), 20 mPa.s (lighter filled circles) and 6.2 mPa.s (open circles)

lowered in this system through the addition of SDS surfactant to the water phase¹⁵. By reducing the concentration of SDS below the critical micelle concentration (CMC), it is possible to increase the interfacial tension relative to the solution with 1% SDS^{7,15,16}. Fig. 4A shows the snap-off droplet radius for three different interfacial tensions at increasing flow rates for the same pipette. Since snap-off is driven by interfacial tension, droplets snap-off sooner at increased interfacial tension for a given flow rate. Smaller droplets are produced as a result, which can be clearly seen in Fig. 4A, where the curves of higher interfacial tension fall below those of lower interfacial tension. Based on previous experiments with different hydrocarbons, we estimate the interfacial tension of mineral oil and water at SDS concentrations of 1%, 0.1%, and 0.05% to be 12 mN/m, 25 mN/m, and 36 mN/m, respectively¹⁶. Interfacial tension is accounted for in the non-dimensionalization of Q , and so Fig. 4B presents the same data as panel A in terms of non-dimensional variables \tilde{R}_d and \tilde{Q} , calculated using the estimated values of γ . The collapsed datasets confirm the role of interfacial tension in rescaling the flow rate.

Previous snap-off studies have investigated the role of the viscosity ratio of dispersed phase to continuous phase, η/η_w ^{5,6}. As with interfacial tension, neither viscosity value is important in the low-flow limit (Eq. 2)^{5,8}. At higher flow rates, Eq. 5 predicts a dependence of droplet size on the viscosity of the dispersed phase only resulting from the Poiseuille flow through the nozzle opening (Eq. 3). This dependence is accounted for in the scaling of $\tilde{Q} \propto \eta Q$, as in the case of interfacial tension, above. Viscosity of the oil phase was reduced by adding dodecane to the mineral oil. Although this change also has some impact on other properties of the oil, such as interfacial tension and density, the change to viscosity is expected to dominate for the purposes of snap-off droplet production. Viscosities of the 25% and 50% solutions of dodecane in mineral oil were calculated as 20 ± 1 mPa.s and 6.2 ± 0.3 mPa.s, respectively^{14,17}. Measurements of these viscosities through Stokes' law agreed with the calculated values. Fig. 4C plots snap-off droplet radius R_d as a function of flow rate Q for three oil phase viscosities ejected from the same pipette. According to Eq. 3, a lower viscosity is associated with a smaller pressure gradient for the same flow rate, as compared to a higher viscosity. A lower viscosity thus increases the relative importance of the Laplace pressure terms in Eq.5 and causes snap-off to occur at flow rates where it otherwise would not. As with interfacial

tension, viscosity of the dispersed phase can be seen as an adjustment to non-dimensionalized flow rate \tilde{Q} .

The theory presented here to describe snap-off (Eq. 5) predicts only the onset of droplet instability. It is assumed that the continuous phase invades the nozzle immediately upon fulfilling the snap-off condition and so the threshold for droplet instability is the same as that for actual snap-off. It is for this reason that the theory fails for a perfectly circular opening, since the continuous phase is unable to flow into the nozzle^{9,11}. This assumption must also fail in the limit of a highly viscous continuous phase. In order to investigate the role of continuous phase viscosity on snap-off droplet production, glycerol was added to the water phase. As with the addition of dodecane to the mineral oil, addition of glycerol to water is expected to alter interfacial tension and density, but the increased viscosity is expected to dominate changes to the snap-off behaviour. The viscosity of the water phase does not affect the size of droplets produced from a single pipette at any flow rate, as seen in Fig. 5A. In order to obtain a higher viscosity of the water phase relative to the oil phase, a 50% solution of dodecane in mineral oil was used as the discontinuous phase for this experiment, with a calculated and measured viscosity of $\eta = 6.2 \pm 0.3$ mPa.s. The viscosity of the continuous phase varied between $\eta_w = 1.0$ mPa.s (0% glycerol) and $\eta_w = 10.8$ mPa.s (60% glycerol)¹⁸. The experiment was also conducted without addition of dodecane to the dispersed phase with similar results. The independence of snap-off on continuous phase viscosity provides justification for using a stability condition as a snap-off condition directly. Furthermore, the viscosity ratio has previously been assumed to be an important parameter for snap-off production, as is the case for other droplet production techniques^{1,4-6}. However, our results suggest that it is only the viscosity of the dispersed phase that is meaningful, not its ratio to the viscosity of the continuous phase, at least over the range of viscosities tested here. To emphasize this point, Fig. 5B presents two datasets from the same pipette with the same viscosity ratio, $\eta/\eta_w = 20$, but different viscosity pairs. The lack of overlap between these two datasets provides direct evidence that the viscosity ratio is not the correct parameter to consider in the context of snap-off droplet production.

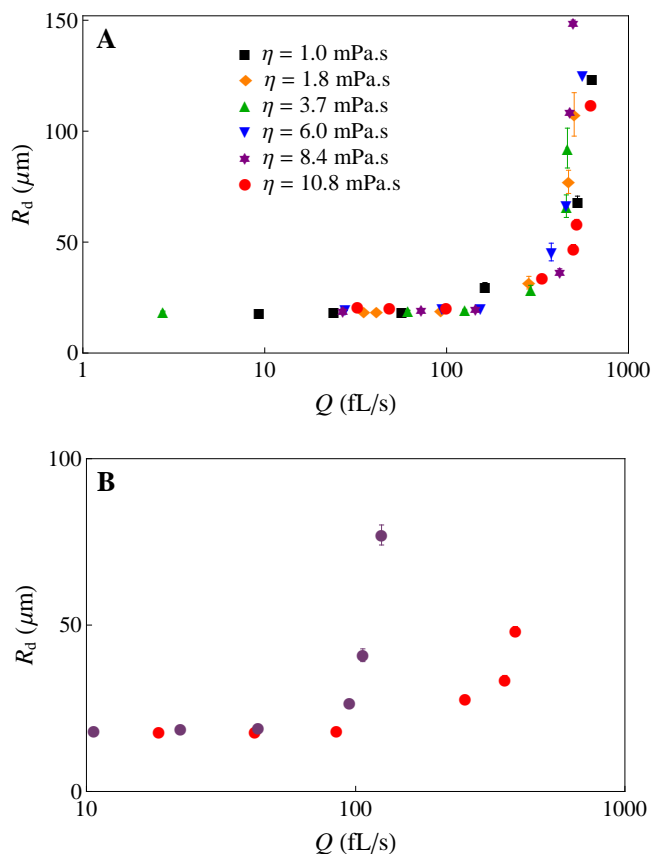


Fig. 5 A) Snap-off droplet sizes produced from a single pipette at increasing flow rates for several viscosities of the continuous phase, from 1 mPa.s (squares) to 10 mPa.s (circles). B) Snap-off droplet sizes produced from a single pipette for two different liquid pairs with the same viscosity ratio $\eta/\eta_w=20$.

5 Conclusions

We have presented a model describing snap-off droplet size over a wide range of flow rates, based on simple arguments of Laplace pressure and Poiseuille flow. Pipette dimensions, interfacial tension, and dispersed phase viscosity are all accounted for. Adjustment of these parameters increases the versatility of droplet production, specifically by increasing the range of flow rates over which droplets can be produced. Interestingly, the continuous phase viscosity has no impact on snap-off over the entire range tested, including cases where the continuous phase is more viscous than the dispersed phase. Although our model was developed for a cylindrical geometry, it should be applicable to all droplet snap-off geometries with appropriate adjustments. The

model predicts a rich and unexpected stability dependence on droplet size and flow rate, which was confirmed experimentally by producing droplets with radii that are normally forbidden for a particular pipette.

References

- 1 A. S. Utada, A. Fernandez-Nieves, H. A. Stone and D. A. Weitz, *Physical review letters*, 2007, **99**, 094502.
- 2 R. Dangla, E. Fradet, Y. Lopez and C. N. Baroud, *Journal of Physics D: Applied Physics*, 2013, **46**, 114003.
- 3 P. Garstecki, M. J. Fuerstman, H. A. Stone and G. M. Whitesides, *Lab on a Chip*, 2006, **6**, 437–446.
- 4 S. Sugiura, M. Nakajima, N. Kumazawa, S. Iwamoto and M. Seki, *The Journal of Physical Chemistry B*, 2002, **106**, 9405–9409.
- 5 K. van Dijke, R. de Ruiter, K. Schroën and R. Boom, *Soft Matter*, 2010, **6**, 321–330.
- 6 T. Peña, M. Carvalho and V. Alvarado, *AIChE journal*, 2009, **55**, 1993–1999.
- 7 S. Sugiura, M. Nakajima, T. Oda, M. Satake and M. Seki, *Journal of colloid and interface science*, 2004, **269**, 178–185.
- 8 R. Dangla, S. C. Kayi and C. N. Baroud, *Proceedings of the National Academy of Sciences*, 2013, **110**, 853–858.
- 9 S. Barkley, E. R. Weeks and K. Dalnoki-Veress, *Eur. Phys. J. E.*, In Press.
- 10 R. Lenormand, C. Zarcone and A. Sarr, *Journal of Fluid Mechanics*, 1983, **135**, 337–353.
- 11 J. Roof *et al.*, *Society of Petroleum Engineers Journal*, 1970, **10**, 85–90.
- 12 S. Sugiura, M. Nakajima and M. Seki, *Langmuir*, 2002, **18**, 5708–5712.
- 13 L. Landau and E. Lifshits, *Course of Theoretical Physics: Fluid Mechanics*, Butterworth-Heinenann, 1987.
- 14 A. S. D7152-11, *Standard practice for calculating viscosity of a blend of petroleum products*, ASTM International, West Conshohocken, PA, 2006.
- 15 J. R. Campanelli and X. Wang, *Journal of colloid and interface science*, 1997, **190**, 491–496.
- 16 S. J. Rehfeld, *The Journal of Physical Chemistry*, 1967, **71**, 738–745.
- 17 D. Caudwell, J. Trusler, V. Vesovic and W. Wakeham, *International Journal of Thermophysics*, 2004, **25**, 1339–1352.
- 18 J. B. Segur and H. E. Oberstar, *Industrial & Engineering Chemistry*, 1951, **43**, 2117–2120.

Chapter 5

Compression of two-dimensional droplet clusters

Crystals and glasses are distinct forms of solid matter, distinguished from one another at a macroscopic scale by their material properties, and at a microscopic scale by the spatial arrangement of individual particles. While crystals are often considered to be perfectly ordered, and glasses to be perfectly disordered, this is an overly simple interpretation. Some crystals have significant disorder at a molecular level, while some glasses have a highly organized structure, particularly at a local scale [34, 35]. These types of observations have prompted recent efforts to characterize systems that are intermediate between crystals and glasses, both in terms of mechanical properties and particle order [26, 36–38].

In addition to ambiguity regarding the transition from crystalline to glassy behaviour, there are also questions regarding the minimum system size for the onset of either of these states [34, 39]. A system composed of only a few molecules cannot be realistically described as either a crystal or a glass, and demonstrates vastly different properties than a bulk system of the same material [39–41]. These confinement effects are thought to be central to developing a theory of glass transitions [24, 39].

Colloidal glasses are some of the most studied systems for investigating the role of disorder in microscopic structure [37, 39, 42]. These systems are analogous to molecular glasses in many ways, but have some important differences. Quantum effects and thermal motion do not influence the motion of 25 μm particles, which is part of the

reason they are more easily visualized than their atomic counterparts. The interaction between individual particles is also different, with colloids typically experiencing both hard-sphere repulsion and hydrodynamic coupling [42]. Soft colloids and emulsions are more versatile in terms of interparticle interactions, as these particles are deformable and do not obey hard sphere repulsion [3, 42–44]. Gravitational forces also play a role in crystallization of colloid systems specifically, but can be avoided by density matching particles to the continuous liquid, or by considering only 2D horizontal systems [42]. 2D systems are also advantageous for imaging and for calculating all forces applied to individual particles by their neighbours [3, 37, 38]

Force measurements play an important role in understanding colloidal crystals or glasses, elucidating behaviour at both the macroscopic and microscopic scale. Macroscopic properties of interest include elastic and shear moduli, packing density, and pressure, while microscopic properties include particle deformation, coordination number, and the distribution of interparticle forces [3, 25, 26, 37, 44]. Unfortunately, both sets of properties are difficult to measure in the case of microscopic emulsions, corresponding to nN forces [3, 44]. Instead of direct measurements, forces are usually inferred from other sources of information, such as particle deformations or particle displacement under a known stress [3, 37, 44].

Here, we present experiments in which 2D droplet clusters are compressed between two thin glass pipettes, and the compressive force is measured directly to sub-nanonewton precision. This setup allows probing of the transition from glassy to crystalline behaviour with increasing droplet monodispersity. Additionally, the number of droplets can be increased from a single pairwise interaction to hundreds of droplets, traversing the mesoscopic scale and permitting investigation of the onset of bulk behaviour. Images of the droplet cluster during compression can be compared with direct force measurements captured through micropipette deflection to associate specific rearrangement events with their corresponding signatures in the force-compression curve. Currently, this project is in preliminary stages. While much work has been done to optimize the experimental setup, more experiments and more sophisticated analysis are required to advance this project towards publication.

Monodisperse droplets ($R \approx 15\mu\text{m}$) were produced from a micropipette via the snap-off method described in chapters 3 and 4. Approximately 20 droplets were

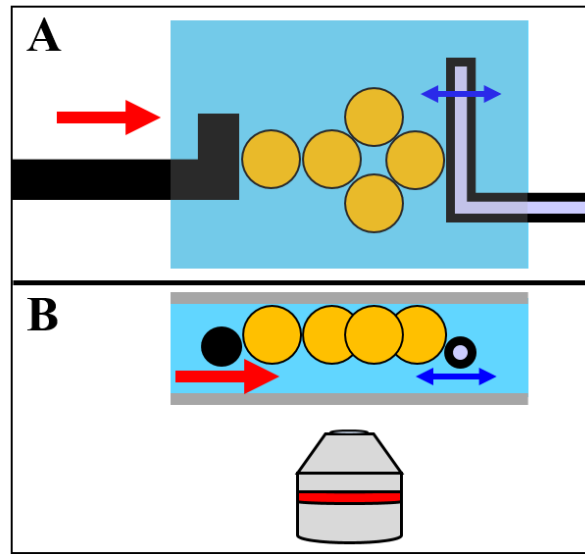


Figure 5.1: Experimental setup for compression of droplet clusters. A) Top view. The stiff pipette on the left is pushed forward at a constant rate, while the flexible pipette on the right deflects in response to applied forces. B) Side View. Droplets float to the top of the sample chamber.

arranged between two more micropipettes of $\approx 10 \mu\text{m}$ radius after floating to the top of the sample chamber, which confined droplets to a 2D geometry (Fig. 5.1B). One of the two pipettes was stiff and was moved forward at a constant rate of 100 nm/s to compress the droplet cluster (Fig. 5.1). This slow rate ensured that hydrodynamic coupling between the pipette and droplets, or between droplets and their neighbours, was negligible. The other pipette was thin and flexible, deflecting laterally in response to an applied force (Fig. 5.1). These deflections, on the order of $1 \mu\text{m}$, were much smaller than the size of the droplets, and so this micropipette acted as an ideal force transducer. Droplets were mineral oil and the aqueous continuous phase contained 1% SDS and 2% NaCl, both by weight in deionized water. Droplets of different sizes were produced by varying the flow rate of mineral oil through the droplet-producing pipette.

A collection of monodisperse droplets forms a perfect 2D crystal, as seen in Fig. 5.2A. Upon compression (by the upper pipette in Fig. 5.2), the crystal is able to withstand some force, as seen by the slight deflection of the lower pipette in Fig. 5.2B. The crystal fractures when the force required to do so is less than that required

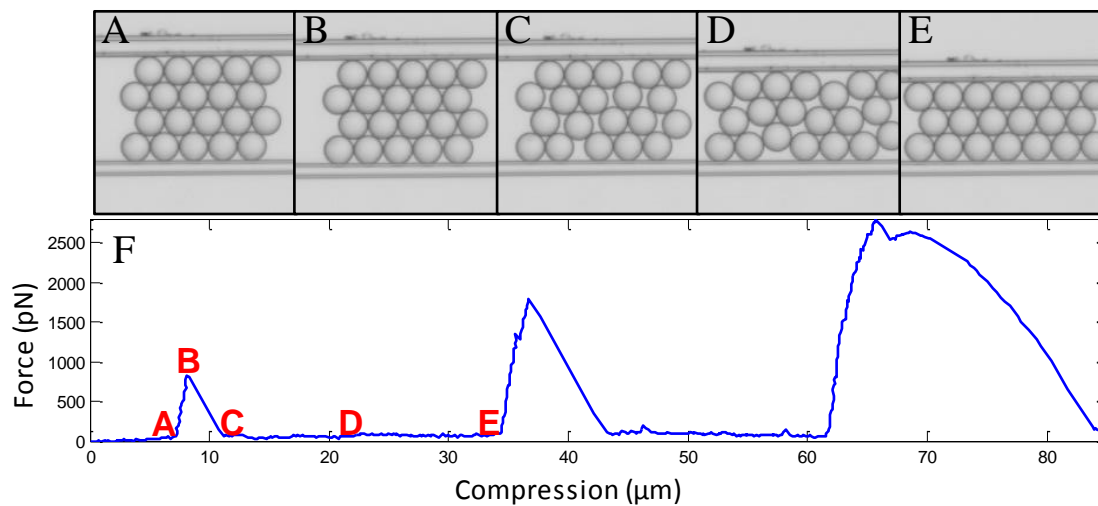


Figure 5.2: Compression of a monodisperse droplet cluster. A) Cluster is crystalline prior to compression. B) The crystal can withstand some force, and the lower flexible pipette deflects. C) Force increases past the breaking point of the crystal, and it fractures. D) The droplets slide easily past one another after breaking apart. E) The droplets eventually achieve a new crystalline configuration. F) Deflection of the lower pipette plotted against cluster compression (blue curve) during the entire experiment. Data points corresponding to the images in panel A-E are indicated by red letters.

to continue deflecting the force-sensing pipette, which returns to its original, undeflected position (Fig. 5.2C). Upon further compression, the droplets slide past one another easily, and no force is transmitted through the structure to the lower pipette (Fig. 5.2D). Eventually, the droplets regain a crystalline arrangement, albeit with one less layer of droplets, pictured in Fig. 5.2E). Position of both pipettes is recorded throughout the experiment and deflection of the lower pipette is used to measure the compressive force, plotted against cluster compression in Fig. 5.2F. The data points corresponding to the images of panels A-E are noted in red. The second peak in Fig. 5.2F at compression = $36 \mu\text{m}$ is due to fracture of the crystal shown in Fig. 5.2E). The system then evolves to a crystal with only two layers, which also fractures at compression = $65 \mu\text{m}$.

Generally, compression of a crystal produces a series of periodic peaks with separation equal to the lattice constant, $\sqrt{3}R$ ($= 29 \mu\text{m}$ in the case presented in Fig. 5.2). Peak height tends to increase over the course of an experiment for several reasons. First, the water solution is constantly evaporating due to the chamber design, de-

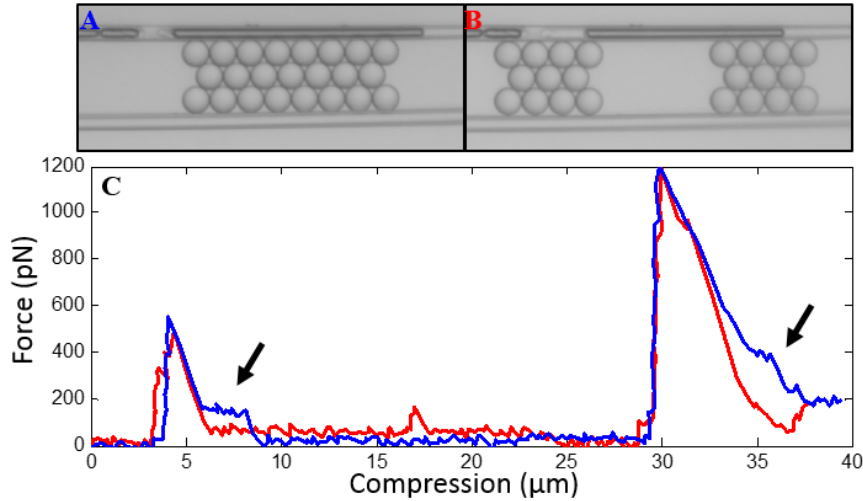


Figure 5.3: Effect of crystal boundaries. A) One large crystal. Upon compression, the droplets can only displace from its ends. B) Two smaller crystals. Upon compression, the droplets can displace from the ends or into the middle of the structure. C) Force-compression curve of the clusters shown in panel A (blue curve) and B (red curve). Black arrows indicate a longer relaxation time of the large crystal as droplets move further.

scribed in section 2.2. This results in a constantly increasing concentration of NaCl, which screens the Coulombic repulsion between droplets. While the evaporated volume is relatively small, the interaction strength is particularly sensitive to even small changes in NaCl concentration and the experiment depicted in Fig. 5.2 took 15 minutes to complete, allowing ample time for some evaporation to occur. While this is an unintended consequence of the sample chamber setup, the other reasons for increasing peak height result directly from droplet rearrangements within the cluster. Subsequent crystal fractures require separation of more droplet pairs, as a larger fraction of all droplets in the system are directly involved in later fractures. For the experiment presented in Fig. 5.2, the first fracture (pictured in panels B-C) required severing of 8 contacts between droplets, while the next two fracture events correspond to severing of 13 and 16 contacts. In addition to the increased attractive interaction between droplets due to evaporation, more droplet pairs must be pulled apart for later fractures to occur. Finally, later fractures require individual droplets to move further as the cluster expands in the direction perpendicular to the applied compression due to conservation of volume (horizontal expansion in Fig. 5.2). Movement of droplets is

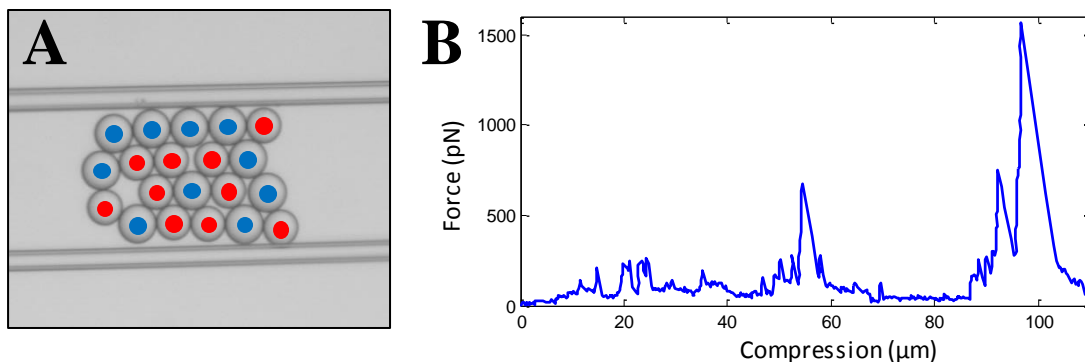


Figure 5.4: Bidisperse droplet cluster, with smaller droplets indicated in red and larger droplets in blue. A) Prior to compression, droplet arrangement is not as well ordered as the monodisperse droplets in Figs. 5.2 and 5.3. B) Force-compression curve of the bidisperse cluster has many irregularly spaced peaks of varying heights due to its chaotic breakup.

hindered by viscous drag, as well as by friction forces of sliding along both the upper coverslip of the sample chamber and pipettes. Figure 5.3 provides evidence of the cost of increased droplet displacement. The droplets in the cluster shown in panel A must move further than those in panel B upon compression, due to the large gap in the cluster in panel B that can be filled with droplets. Although the magnitude of the force peaks required to fracture each crystal is similar (Fig. 5.3C, red and blue curves), it takes much longer for the cluster shown in panel A (blue data) to return to a relaxed configuration (elevated force indicated by black arrows in Fig. 5.3C). This result is reproducible, and suggests that although the need for increased droplet movement may not contribute to the force required for an initial crystal fracture, it does contribute to the relaxation of the fractured crystal.

Bidisperse droplet clusters with an arbitrary radius ratio cannot form perfect crystals, but instead form glasses [3, 38]. Although the droplets may be arranged in a similar configuration to those in a crystalline cluster (Fig. 5.4A vs. Fig. 5.2A), not all neighbouring droplets are in contact in the bidisperse case, resulting in considerable structural disorder. Upon compression, the cluster behaviour is noticeably different. Instead of large periodic peaks of increasing amplitude, as in Figs. 5.2F or 5.3C, the force transmitted through the bidisperse cluster appears as many smaller peaks of varying height (Fig. 5.4B). It is important to note that this random signal is not

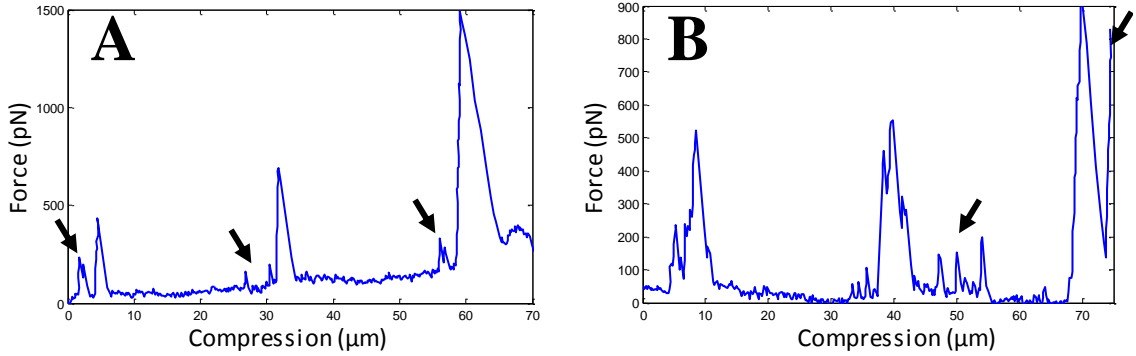


Figure 5.5: Force curves of droplet clusters containing single defects. A) A single droplet larger than the others in the clusters causes one region of the crystal to locally fracture at lower compression than the rest of the crystal, indicated by black arrows. B) if the defect droplet is abnormally small, it shifts fracture to a higher compression, indicated by black arrows.

experimental noise. The noise threshold is visible in Fig. 5.4B between compression of $70 - 85 \mu\text{m}$, and is approximately 15 pN . Each of the larger peaks with amplitude $\geq 100 \mu\text{m}$ correspond to the breaking of one or more contacts between droplets. Rather than undergoing a few large rearrangements due to fracture and dislocation of crystal layers in response to compression, the glassy system relaxes in a much more continuous manner through several smaller rearrangements. Frequently, resolution of one jamming location does not relieve very much stress, and the force does not return to its baseline value (Fig. 5.4). This is because the system's evolution is chaotic and the motion of distant particles is uncorrelated, even across this relatively small cluster. As in the monodisperse case, amplitude of force peaks does tend to increase over the course of an experiment due to evaporation, the need to break more contacts, and the need for increased droplet movement. However, small peaks persist into the late stages of cluster compression as a result of minor rearrangements that require breaking only one or a few contacts between droplets.

Finally, a set of experiments were performed to probe the transition from glassy to crystalline behaviour. A single mismatched droplet was introduced to a cluster of monodisperse droplets. This resulted in behaviour that was intermediate between that of the monodisperse (crystalline) case and that of the bidisperse (glassy) case. Specifically, the portion of the crystal containing the defect fractured separately from

the rest of the crystal, resulting in splitting of the periodic peaks that are characteristic of compressing a monodisperse droplet cluster. In the case of a single droplet that was larger than its neighbours, lower compression was required for local fracture, and peaks are observed before the main peak for each rearrangement (Fig. 5.5A). Similarly, a single small droplet requires higher compression and results in satellite peaks after the main, periodic peak (Fig. 5.5B).

These preliminary results of monodisperse, bidisperse, and defected clusters demonstrate the promise of this experimental system for investigating the role of disorder and system size on glassy and crystalline dynamics. Force measurements by pipettes are bulk system measurements. However, due to the mesoscopic system size, they can be associated with individual rearrangement events within the cluster. Microscopic parameters are also accessible from the image sequences, including coordination number, bond orientation, and velocity of individual particles. Ongoing efforts aim to associate these parameters with the measured force curves to increase understanding of the relative magnitudes of forces within an experiment.

Chapter 6

Conclusions

Emulsions are an active area of research, primarily for their use in microfluidics and as model systems to investigate glass formation and other molecular phenomena. Both of these applications require methods to reliably produce highly monodisperse droplets. We introduced the snap-off technique to produce droplets from micropipettes, with a higher monodispersity than is attainable through other methods. In the tips and tricks paper (chapter 3), we also demonstrate some of its other advantages, including versatility, cost effectiveness and ease of use. Next, we explored the mechanism of this method, providing a thorough understanding of why the droplets break off at particular sizes, and giving other researchers additional tools to use this method effectively. However, the primary motivation for the second paper (chapter 4) was to investigate the science behind snap-off, not to improve its use as an experimental technique.

Monodisperse droplets were needed for micropipette deflection experiments on compression of 2D droplet clusters. Currently, this project is in its preliminary stages. While experimental details and methods have been finalized, analysis remains an ongoing challenge. Once the analysis procedure has been optimized, this set of experiments represents an ideal system to probe the transitions from isolated particles to bulk crystals and glasses. The direct force measurements from micropipette deflection provide a valuable tool to probe system evolution during compression. While the image analysis and associated interpretation is not a trivial task, it should be relatively straightforward to extract the necessary information from the experiments

to quantitatively characterize their differing breakup patterns.

The experimental setup developed for this project can also accommodate many additional experiments. Immediate extensions include increasing the size of clusters or changing the size ratio of droplets in bidisperse clusters without requiring any adjustments to the experimental setup. With modifications to pipette geometry, the same techniques presented here could be used to investigate the deformation of droplet clusters under shear or tension, in addition to compression. Additionally, there are several larger modifications that could be made to the experiment to probe entirely different physics. If the interaction strength between droplets is increased, or if droplets are density-matched to the continuous phase, then buoyancy will not restrict droplets to the upper surface of the chamber and they will form 3D clusters, which are interesting in their own right. The smallest droplets produced by the snap-off method are affected by thermal agitation. This vastly increases the depth of comparisons to molecular systems. For example, a long chain of small droplets bound to pipettes at either end could be used to model a short polymer molecule acting as an entropic spring. Finally, the mineral oil droplets could be replaced with polymerosomes or lipid vesicles to investigate problems relating to diffusion and vesicle fusion. Each of these potential projects presents its own challenges, but the experimental methods I developed during my master's research provide a strong foundation from which to begin. This contribution to future research is perhaps the most important outcome of the work described in this thesis.

Bibliography

- [1] Koen C van Dijke, Karin Schroën, Albert van der Padt, and Remko Boom. Edge emulsification for food-grade dispersions. *Journal of food engineering*, 97(3):348–354, 2010.
- [2] JG Roof et al. Snap-off of oil droplets in water-wet pores. *Society of Petroleum Engineers Journal*, 10(01):85–90, 1970.
- [3] Kenneth W Desmond, Pearl J Young, Dandan Chen, and Eric R Weeks. Experimental study of forces between quasi-two-dimensional emulsion droplets near jamming. *Soft Matter*, 9(12):3424–3436, 2013.
- [4] Jan Guzowski and Piotr Garstecki. Droplet clusters: Exploring the phase space of soft mesoscale atoms. *Physical review letters*, 114(18):188302, 2015.
- [5] P.G. de Gennes, F. Brochard-Wyart, and D. Quere. *Capillarity and Wetting Phenomena: Drops, Bubbles, Pearls, Waves*. Springer, 2004.
- [6] Kevin B Strawbridge, Erin Ray, F Ross Hallett, Susan M Tosh, and Douglas G Dalgleish. Measurement of particle size distributions in milk homogenized by a microfluidizer: estimation of populations of particles with radii less than 100 nm. *Journal of Colloid and Interface Science*, 171(2):392–398, 1995.
- [7] Robert Jenness, Ernest O Herreid, WJ Caulfield, LH Burgwald, EL Jack, and SL Tuckey. The density of milk fat: its relation to the accuracy of the babcock test. *Journal of Dairy Science*, 25(11):949–960, 1942.

-
- [8] Selwyn J Rehfeld. Adsorption of sodium dodecyl sulfate at various hydrocarbon-water interfaces. *The Journal of Physical Chemistry*, 71(3):738–745, 1967.
- [9] John R Campanelli and Xiaohong Wang. Effect of neck formation on the measurement of dynamic interfacial tension in a drop volume tensiometer. *Journal of colloid and interface science*, 190(2):491–496, 1997.
- [10] Samuel Levine, Bruce D Bowen, and Susan J Partridge. Stabilization of emulsions by fine particles ii. capillary and van der waals forces between particles. *Colloids and surfaces*, 38(2):345–364, 1989.
- [11] Rémi Dangla, S Cagri Kayi, and Charles N Baroud. Droplet microfluidics driven by gradients of confinement. *Proceedings of the National Academy of Sciences*, 110(3):853–858, 2013.
- [12] Takasi Nisisako, Toru Torii, Takanori Takahashi, and Yoichi Takizawa. Synthesis of monodisperse bicolored janus particles with electrical anisotropy using a microfluidic co-flow system. *Advanced Materials*, 18(9):1152–1156, 2006.
- [13] Christian Holtze. Large-scale droplet production in microfluidic devices an industrial perspective. *Journal of Physics D: Applied Physics*, 46(11):114008, 2013.
- [14] Gary L Hunter, Kazem V Edmond, and Eric R Weeks. Boundary mobility controls glassiness in confined colloidal liquids. *Physical Review Letters*, 112(21):218302, 2014.
- [15] Eric Brouzes, Martina Medkova, Neal Savenelli, Dave Marran, Mariusz Twardowski, J Brian Hutchison, Jonathan M Rothberg, Darren R Link, Norbert Perimon, and Michael L Samuels. Droplet microfluidic technology for single-cell high-throughput screening. *Proceedings of the National Academy of Sciences*, 106(34):14195–14200, 2009.
- [16] KF Clifton et al. An integrated microfluidic device for large-scale in situ click chemistry screening. *Lab on a Chip*, 9(16):2281–2285, 2009.
- [17] Peng Liu and Richard A Mathies. Integrated microfluidic systems for high-performance genetic analysis. *Trends in biotechnology*, 27(10):572–581, 2009.

- [18] Andrew S Utada, Alberto Fernandez-Nieves, Howard A Stone, and David A Weitz. Dripping to jetting transitions in coflowing liquid streams. *Physical review letters*, 99(9):094502, 2007.
- [19] JH Xu, SW Li, J Tan, YJ Wang, and GS Luo. Preparation of highly monodisperse droplet in a t-junction microfluidic device. *AIChE journal*, 52(9):3005–3010, 2006.
- [20] Piotr Garstecki, Michael J Fuerstman, Howard A Stone, and George M Whitesides. Formation of droplets and bubbles in a microfluidic t-junction: scaling and mechanism of break-up. *Lab on a Chip*, 6(3):437–446, 2006.
- [21] Koen van Dijke, Riëlle de Ruiter, Karin Schroën, and Remko Boom. The mechanism of droplet formation in microfluidic edge systems. *Soft Matter*, 6(2):321–330, 2010.
- [22] Shinji Sugiura, Mitsutoshi Nakajima, Naoyuki Kumazawa, Satoshi Iwamoto, and Minoru Seki. Characterization of spontaneous transformation-based droplet formation during microchannel emulsification. *The Journal of Physical Chemistry B*, 106(36):9405–9409, 2002.
- [23] V Trappe, V Prasad, Luca Cipelletti, PN Segre, and DA Weitz. Jamming phase diagram for attractive particles. *Nature*, 411(6839):772–775, 2001.
- [24] Thomas Salez, Justin Salez, Kari Dalnoki-Veress, Elie Raphaël, and James A Forrest. Cooperative strings and glassy interfaces. *Proceedings of the National Academy of Sciences*, 112(27):8227–8231, 2015.
- [25] Corey S O’Hern, Stephen A Langer, Andrea J Liu, and Sidney R Nagel. Force distributions near jamming and glass transitions. *Physical review letters*, 86(1):111, 2001.
- [26] Carl P Goodrich, Andrea J Liu, and Sidney R Nagel. Solids between the mechanical extremes of order and disorder. *Nature Physics*, 10(8):578–581, 2014.
- [27] J.N. Israelachvili. *Intermolecular and Surface Forces*. Intermolecular and Surface Forces. Elsevier Science, 2010.

-
- [28] Raymond R Dagastine, Geoffrey W Stevens, DYC Chan, and Franz Grieser. Forces between two oil drops in aqueous solution measured by afm. *Journal of colloid and interface science*, 273(1):339–342, 2004.
- [29] M-J Colbert, AN Raegen, C Fradin, and K Dalnoki-Veress. Adhesion and membrane tension of single vesicles and living cells using a micropipette-based technique. *The European Physical Journal E*, 30(2):117–121, 2009.
- [30] John M Frostad, Martha C Collins, and L Gary Leal. Cantilevered-capillary force apparatus for measuring multiphase fluid interactions. *Langmuir*, 29(15):4715–4725, 2013.
- [31] Vernita D Gordon, Xi Chen, John W Hutchinson, Andreas R Bausch, Manuel Marquez, and David A Weitz. Self-assembled polymer membrane capsules inflated by osmotic pressure. *Journal of the American Chemical Society*, 126(43):14117–14122, 2004.
- [32] Rafael D Schulman, Matilda Backholm, William S Ryu, and Kari Dalnoki-Veress. Dynamic force patterns of an undulatory microswimmer. *Physical Review E*, 89(5):050701, 2014.
- [33] Matilda Backholm, William S Ryu, and Kari Dalnoki-Veress. Viscoelastic properties of the nematode *caenorhabditis elegans*, a self-similar, shear-thinning worm. *Proceedings of the National Academy of Sciences*, 110(12):4528–4533, 2013.
- [34] Michael V Massa, Jessica L Carvalho, and Kari Dalnoki-Veress. Confinement effects in polymer crystal nucleation from the bulk to few-chain systems. *Physical review letters*, 97(24):247802, 2006.
- [35] P. H. Gaskell and D. J. Wallis. Medium-range order in silica, the canonical network glass. *Phys. Rev. Lett.*, 76:66–69, Jan 1996.
- [36] M. Hanifpour, N. Francois, S. M. Vaez Allaei, T. Senden, and M. Saadatfar. Mechanical characterization of partially crystallized sphere packings. *Phys. Rev. Lett.*, 113:148001, Oct 2014.

-
- [37] Nathan C Keim and Paulo E Arratia. Role of disorder in finite-amplitude shear of a 2d jammed material. *Soft matter*, 11(8):1539–1546, 2015.
- [38] Peter Yunker, Zexin Zhang, and A. G. Yodh. Observation of the disorder-induced crystal-to-glass transition. *Phys. Rev. Lett.*, 104:015701, Jan 2010.
- [39] Carolyn R. Nugent, Kazem V. Edmond, Hetal N. Patel, and Eric R. Weeks. Colloidal glass transition observed in confinement. *Phys. Rev. Lett.*, 99:025702, Jul 2007.
- [40] Nicolas Giovambattista, Peter J. Rossky, and Pablo G. Debenedetti. Phase transitions induced by nanoconfinement in liquid water. *Phys. Rev. Lett.*, 102:050603, Feb 2009.
- [41] M Beiner, GT Rengarajan, S Pankaj, D Enke, and M Steinhart. Manipulating the crystalline state of pharmaceuticals by nanoconfinement. *Nano letters*, 7(5):1381–1385, 2007.
- [42] Gary L Hunter and Eric R Weeks. The physics of the colloidal glass transition. *Reports on Progress in Physics*, 75(6):066501, 2012.
- [43] Peter J Yunker, Ke Chen, Matthew D Gratale, Matthew A Lohr, Tim Still, and AG Yodh. Physics in ordered and disordered colloidal matter composed of poly (n-isopropylacrylamide) microgel particles. *Reports on Progress in Physics*, 77(5):056601, 2014.
- [44] Jasna Brujić, Sam F Edwards, Dmitri V Grinev, Ian Hopkinson, Djordje Brujić, and Hernán A Makse. 3d bulk measurements of the force distribution in a compressed emulsion system. *Faraday discussions*, 123:207–220, 2003.